Chemical Engineering Journal Advances 16 (2023) 100521

Contents lists available at ScienceDirect

Chemical Engineering Journal Advances

journal homepage: www.sciencedirect.com/journal/chemical-engineering-journal-advances

Prediction of tar yield produced from devolatilisation of empty fruit bunch in a fluidised-bed reactor using pseudo-equilibrium model

Mohamad Syazarudin Md Said *, A.M.A Ahmed, Salmiaton Ali, Thomas Choong Shean Yaw, Wan Azlina Wan Ab Karim Ghani

Sustainable Process Engineering Research Center, Department of Chemical and Environmental Engineering, Faculty of Engineering, Universiti Putra Malaysia, 43400 Serdang, Selangor Darul Ehsan, Malaysia

ARTICLE INFO

Keywords:
Pyrolysis
Biomass
Model
Equilibrium-pseudo model
Kinetic
Fluidised-bed

ABSTRACT

In this work, a pseudo-equilibrium model (PEM) is developed for prediction of yield and product from devolatilisation of empty fruit bunch (EFB). The yield of individual species (H_2, CO, CO_2, CH_4, bio-oil, tar, and char) from the primary decomposition of EFB is expressed empirically. Subsequently, they are the inputs to the secondary reaction region. In the secondary reactions zone, the water-gas shift reaction (WGSR) is treated under equilibrium conditions, but kinetically modified by a factor to predict the concentration of the four gases (H_2, CO, CO_2, and H_2O) which participated in this reaction. Meanwhile, the methane, bio-oil and tar are modelled separately in a purely kinetic environment by applying a plug flow reactor (PFR) model to estimate the conversion of both species. The model is further to investigate the effects of changes in the operating conditions of devolatilisation such as temperature and carrier gas flow rate. The results showed a good prediction for tar yield with low root mean square (RMS = 0.003) compared to experiments, and conversion (59.7%) compared to experiments (51.5%) at 850 °C. A sensitivity analysis for the pyrolysis model was conducted to investigate the effects of process temperature and nitrogen gas flowrate. Tar yield was significantly reduced at high temperatures. Meanwhile, the change of nitrogen flowrate resulted in slight increase of tar yield. Reasonable predictions were obtained for other products.

1. Introduction

Tar is a by-product which is produced inevitably in thermal conversion processes such as gasification and pyrolysis (or devolatilisation) at high temperature. This complex product is a condensable organic mixture consists mainly of oxygenated hydrocarbons, typically contains single-ring to five-ring aromatic hydrocarbons [1]. The tar components can be identified through splitting the tar into four classes according to the temperature and residence time as the main criteria for classification [2]. Class 1 comprises the heaviest tars and released at low temperature (500 °C) such as levoglucosan, hydroxyacetaldehyde and furfural [3]. Class 2 is produced in the range of 500 – 1000 °C, and mainly comprises phenolics and olefins. Class 3 consists of alkyl tertiary products (methyl derivatives of aromatics, such as toluene and indene), formed at between 650 and 1000 °C. Class 4 is for the aromatic compounds without substituents such as benzene, naphthalene, anthracene and pyrene, which are formed above 750 °C [4]. At severe gasification conditions (very high temperature), the tar converts to refractory tar which hard to destroy compared to primary and secondary tars due to increase in polymerisation reactions tendency [5]. The tar formation can cause blocking in downstream equipment such as gas coolers, filter elements, pipes, valves, heat exchangers and engine suction channels, and cause catalyst deactivation. Moreover, adherence problems appear on turbine blades, and tar also considered as a corrosive material. As a result, the total efficiency is decreased and the cost of the process is increased. Hence, it is substantial to estimate the tar levels (or concentration) before using syngas as a fuel in internal combustion engine (ICE) which has tolerance for tar. Therefore, the reduction of tar concentration in the syngas is an essential goal for production of clean energy.

Due to complexities of devolatilisation mechanism which consist of many non-elementary reactions, equilibrium model (EM) is adopted in many published works for preliminary estimation of gas composition [6, 7]. This model assumes that equilibrium is reached in the outlet streams since the devolatilisation takes place rapidly. At equilibrium, the system

* Corresponding author.
E-mail address: syazarudin@upm.edu.my (M.S. Md Said).

https://doi.org/10.1016/j.ceja.2023.100521

Available online 14 June 2023

attained more stable composition when its Gibbs free energy is minimised. In fact, the equilibrium is not achieved under practical conditions due to low temperature used in fluidised-bed gasifier between 700 and 900 °C, where extreme conditions required for water-gas shift reaction (WGSR) to reach equilibrium (above 1000 °C). As a result, EM predicts gas composition free of CH_4, tar, and char. In addition, the model overestimates the yields of H_2 and CO, and underestimate the yield of CO_2 [4]. The formation and destruction of tar are not predictable using EM [8]. Unlike equilibrium calculations, pseudo-equilibrium model (PEM) has better results compared to EM. It improves the predictions through inclusion of empirical correlations and kinetic models of kinetically limited-conversion products such as tar, bio-oil, and CH_4 as well as correction factor for WGSR deviation from equilibrium. Moreover, this model allows solid carbon, tar, and CH_4 to be included in the outlet stream. The model is capable to capture the changes in the operating conditions of devolatilisation such as temperature and carrier gas flow rate. In addition, the model is capable to estimate the carbon and WGSR conversions as part of the model rather than being as inputs.

Investigation of tar conversion in biomass pyrolysis through steam reforming reaction is reported in [9,10] where the authors modelled the tar as toluene due to its formation at high temperatures. The approach of thermodynamic equilibrium based on Gibbs free energy was used to study the effects of temperature range (923 – 1273 K) and S/C ratio (steam/carbon molar ratio) between 1 and 4 on the distribution of the products formed from the steam reforming reaction. In this study, 10 species were taken into account as a result of toluene decomposition: methane (CH_4), carbon monoxide (CO), carbon dioxide (CO_2), hydrogen (H_2), ethane (C_2H_6), ethylene (C_2H_4), benzene (C_6H_6), phenol (C_6H_6O), naphthalene ($C_{10}H_8$) and styrene (C8H8). The results of thermodynamic calculations showed that H_2, CO, CO_2 and CH_4 were the main products of the decomposition, while the yield of C_7H_8, $C_{10}H_8$, C_2H_6, C_2H_4, C_6H_6, C_6H_6O, and C_8H_8 were undetectable because they are not thermodynamically favourable species. Thus, constraint conditions on carbon element for the hydrocarbon compounds was introduced. In other words, the carbon in CO, CO_2, and CH_4 was deducted from the total carbon available in the system. As a result, the yield of the produced char was not predicted, which implicitly included in the hydrocarbons. In fact, the produced char in the pyrolysis is very important for successive reactions in gasification, which occupies around 10 wt% of the original biomass. Another study for modelling a downdraft gasifier is reported in [11]. The authors applied a modified equilibrium model through imposing an equilibrium correction for the WGSR and methane formation reactions. The predictions of H_2 and CH_4 improved compared to normal equilibrium approach. In fact, the yield of H_2 decreased while that of CH_4 increased due to correction effects. The results were validated against experimental data at high equivalence ratio (ER = 0.41) in order to satisfy the mole percentage of N_2, consequently, higher amount of air was required in the model proposed. The modified model did not predict the yield of tar and char.

Therefore, in this work, a pseudo-equilibrium model (PEM) is developed for prediction of yield and product from devolatilisation of empty fruit bunch (EFB). In particular, the yield of individual species (H_2, CO, CO_2, CH_4, bio-oil, tar, and char) from the primary decomposition of EFB is expressed empirically. Subsequently, they are the inputs to the secondary reaction region. In the secondary reactions zone, the water-gas shift reaction (WGSR) is treated under equilibrium conditions, but kinetically modified by a factor to predict the concentration of the four gases (H_2, CO, CO_2, and H_2O) which participated in this reaction. Meanwhile, the methane, bio-oil and tar are modelled separately in a purely kinetic environment by applying a plug flow reactor (PFR) model to estimate the conversion of both species. The model is further to investigate the effects of changes in the operating conditions of devolatilisation such as temperature and carrier gas flow rate.

2. Methodology

2.1. Model approach

In this research, the PEM of pyrolysis was represented by decoupling the devolatilisation stage from the secondary reactions. In particular, the yield of individual species (H_2, CO, CO_2, CH_4, bio-oil, tar, and char) from the primary decomposition of EFB is expressed empirically. Subsequently, they are the inputs to the secondary reaction region. In the secondary reactions zone, the WGSR is treated under equilibrium conditions, but kinetically modified by a factor to predict the concentration of the four gases (H_2, CO, CO_2, and H_2O) which participated in this reaction. Meanwhile, the methane, bio-oil and tar are modelled separately in a purely kinetic environment by applying a PFR reactor model to estimate the conversion of both species. Char that formed earlier in the primary decomposition stage remained constant. In other words, this char exists in the model without interaction with other species. In sum, the PEM is to subtract the elemental composition (carbon, hydrogen, and oxygen) of unconverted methane, bio-oil, and tar as well as char from the elemental composition of the gas species released during devolatilisation. As an illustration, the scheme of the reactions is shown in Fig. 1.

The pyrolysis of EFB is a very complex and rapid process. Many pyrolysis models are represented by equilibrium models (EMs) that assume instantaneous equilibrium. In addition, these models employ different pyrolysis mechanisms and product lumps due to EFB's complex structure.

In fact, the equilibrium is not achieved for a water-gas shift reaction (WGSR), the main gas species reaction, unless a catalyst is used. Moreover, methane and tar reactions are kinetically limited. Generally, almost all components of the gas outlet stream are considered at their maximum predicted values [4]. Despite these drawbacks, the EM is still capable of offering initial predictions.

Due to the complexities of the fluidisation regime and segregation issues regarding the two materials (sand and EFB), which differ in their physical properties and shapes, the approach of PEM was applied in a top-feeding reactor, where the EFB free fall on top of the sand bed from a distance of 46 cm. The model employed the kinetic of EFB's primary decomposition, bio-oil, tar, and methane along with yield correlations for gases species from a devolatilisation reaction.

The devolatilisation reaction zone was decoupled from the secondary reactions zone of WGSR, methane, bio-oil, and tar, where the former zone was for the primary decomposition of EFB, as presented in Fig. 2. The devolatilisation area was assumed to be an inert environment (free of O_2) since the gasifying agent has a little impact because of the fast release of volatiles [4]. Even for the secondary reactions zone, which represents the freeboard (FB) of the reactor, it was assumed to be free of O_2 due to rapid consumption of O_2 by the generated char from the primary decomposition of EFB. In fact, the CO_2 reaction is the fastest amongst all char reactions [12]. Moreover, no interactions between carbon and other components (H_2 and CO_2) were considered since the produced char moves downward into the sand bed due to density difference during the encountering with the upward air [4].

2.1.1. EFB chemical formula

The chemical formula of EFB was estimated from its ultimate analysis. In fact, the resulted formula neglects the amount of S and N due to their limited availability in the original biomass. Eventually, the formula comprised only the main components (C, H, and O). This formula was later used in successive calculations in the model, especially in constructing the chemical equation of the EFB decomposition, and the species atomic balance equation.

2.1.2. EFB decomposition chemical equation

The decomposition of EFB is very complex, due to the enormous number of chemical compounds produced simultaneously from different

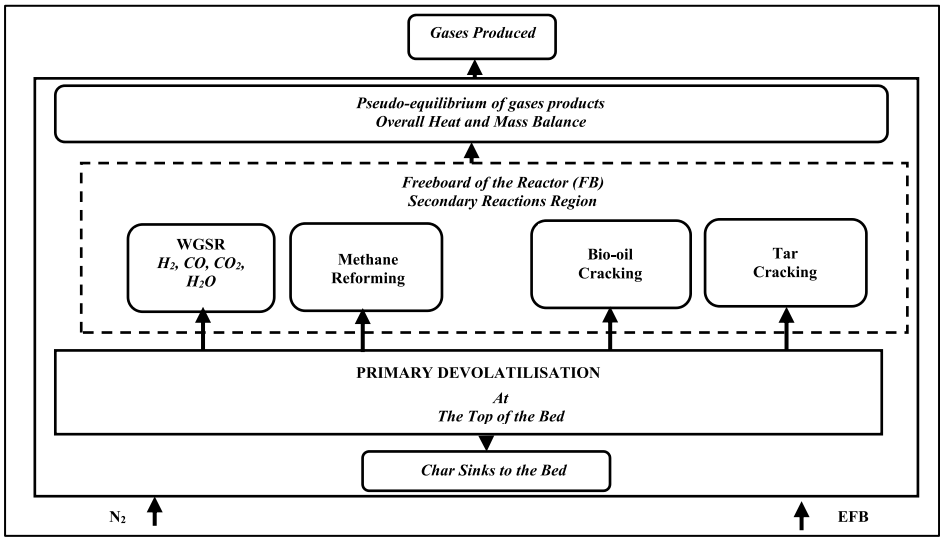

Fig. 1. Flow of reactions in devolatilization pseudo-equilibrium model.

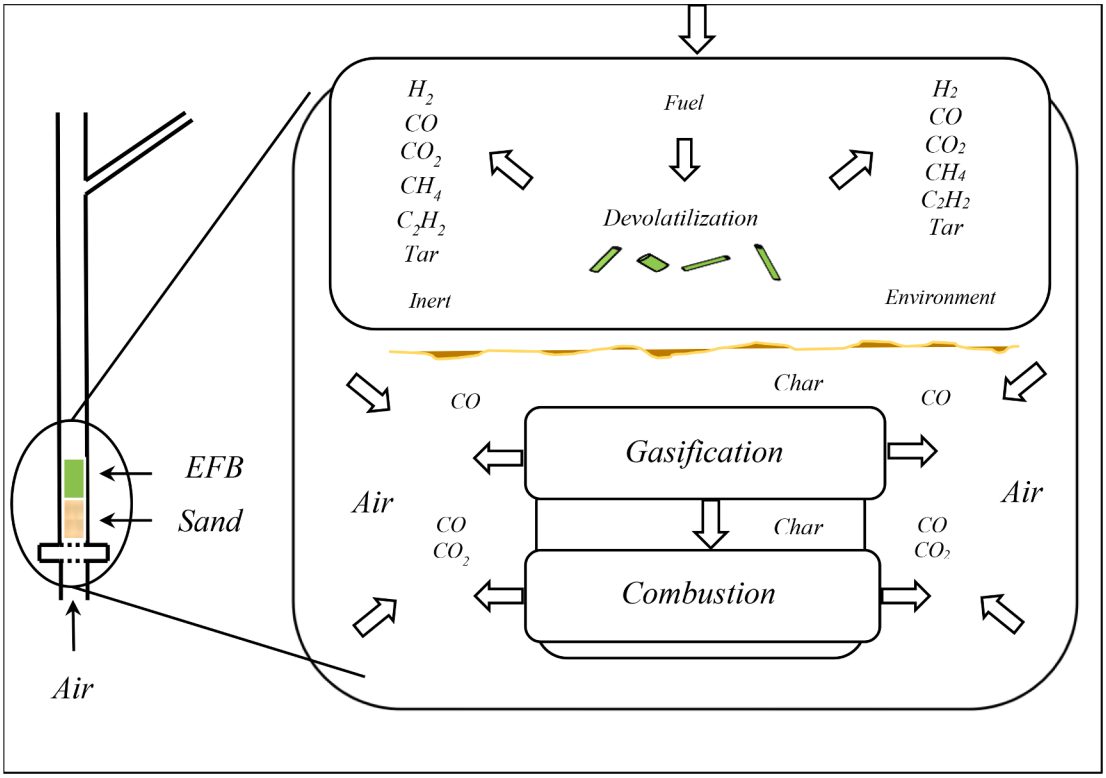

Fig. 2. The sequence of operations in a pyrolyser/gasifier fluidised-bed reactor.

mechanisms at different rates [13]. The mechanism of decomposition is expressed in different ways by many models. In other words, it can be represented as a single, serial, or parallel reaction mechanism in order to describe the primary decomposition and secondary reactions.

In this research, the primary decomposition of the EFB is represented by a single reaction mechanism that results in light gases, bio-oil, tar, water, and char, which can be written as below:

$$biomass \rightarrow (Y_p)_{H_2} H_2 + (Y_p)_{CO} CO + (Y_p)_{CO_2} CO_2 + (Y_p)_{CH_4} CH_4 + (Y_p)_{H_2O} H_2O + (Y_p)_{C_6H_5OH} C_6H_5OH + (Y_p)_{C_7H_8} C_7H_8 + (Y_p)_C C \quad (3)$$

where Y_p refers to the yield of the correspondent species.

In Eq. (3), two component models represented the tar and bio-oil. For tar, toluene (C_7H_8) was chosen because it is a secondary tar evolved at temperature above 650 °C while phenol (C_6 H_6O) is the most abundant component in the bio-oil. Although the tar and bio-oil have a large number of components, only a few are considered in modelling due to lack of availability in kinetic data. The estimation of yield for each individual species was based on chemical reaction stoichiometry (CRS) approach [14]. In general, this approach was used in equilibrium reactions, where the constraints on optimisation were calculated in terms of composition. These constraints can be helpful in solving initial guess problems.

2.1.3. Species thermodynamic properties

The thermodynamic properties of the species (H_2, CO, CO_2, CH_4, H_2O, and N_2) considered in the model were adopted from the online NIST-JANAF thermochemical tables [15]. For examples, heat capacities (Cp^o, J/K. mol) and enthalpies of formation (H_f, kJ/mol) are typical properties used in this model.

On the other hand, the thermodynamic properties for EFB are calculated from empirical equations that depend on the heating value of the biomass itself. In particular, the enthalpy of formation of biomass ($h_{f,EFB}{}^o$, kJ/kg EFB) is the only thermodynamic property required in the PEM, and it can be calculated according to the equation below [16]:

$$h_{f,EFB}{}^o = LHV_{EFB} + \sum_k n_k \, h_{f,k}{}^o \tag{4}$$

where LHV_{EFB} is the lower heating value of EFB (kJ/ kg EFB), v_k represents the stoichiometric coefficient of the product (k) under complete combustion of EFB, and $h_{f,k}{}^o$ (kJ/mol) refers to the enthalpy of formation of the product (k) from the complete combustion of the EFB.

In order to estimate the LHV_{EFB}, the higher heating value of the EFB (HHV_{EFB}, kJ/kg EFB) should be determined first, according to the equation below [17]:

$$HHV_{EFB} = 0.3491C + 1.1783H + 0.1005S - 0.1034O - 0.0151N^* - 0.0211A'' \tag{5}$$

where C, H, S, O, N*, and A" denote the mass percentage of carbon, hydrogen, sulfur, oxygen, nitrogen, and ash in dry basis (db) EFB, respectively.

Subsequently, the LHV_{EFB} is calculated as shown below [12]:

$$LHV_{EFB} = HHV_{EFB} - h_g \left(\frac{9H'}{100} + \frac{M}{100}\right) \tag{6}$$

where h_g represents the latent heat of steam (2260 kJ/kg), and H' and M are the percentage of hydrogen and moisture on an as-received basis, respectively.

Finally, in order to estimate the enthalpy of formation of EFB, the stoichiometric coefficients in Eq. (4) are required. These coefficients represent the stoichiometric coefficients of CO_2 and H_2O, which are the products of complete combustion of the EFB, as shown below:

$$C_pH_jO_h + \left(p + \frac{j}{4} - \frac{h}{2}\right)O_2 \rightarrow p\ CO_2 + \left(\frac{j}{2}\right)H_2O \tag{7}$$

where $C_pH_jO_h$ is the chemical formula of EFB. The variables p, j, and h are the number of atoms of carbon, hydrogen, and oxygen in the EFB, respectively.

In addition to the previously mentioned species, the consideration of specific enthalpies (h^o, kJ/kg) of C_6H_6O, C_7H_8, and carbon are equally important to the thermodynamic properties of EFB and gas species due to their use in energy conservation equation. In particular, these enthalpies are also determined from their elemental composition and heating value. In order to calculate the specific enthalpy for carbon (h °C), an assumption has been made; that is, the produced char consists mainly of pure carbon since the analysis of char is not available, and its ash content is small. Hence, the char is treated as a graphite [18]. Moreover, the LHV and HHV of pure carbon are identical because of the absence of water formation during the combustion of the carbon. A value of 32.8 MJ/kg was adopted as the HHV of carbon; consequently, the same value holds for LHV [19]. Under those circumstances, the specific enthalpy of carbon is obtained by the following equation [18]:

$$h_C^o = H_C - \left[\frac{x_{char}}{M_{Ch}}\right] M_{O2} h_{O2}^o \frac{x1_{char}}{x1_{char} + 2_{ash}} + \left[\frac{x_{char}}{M_{Ch}} M_{CO2} h_{CO2}^o\right] \frac{x1_{char}}{x1_{char} + x2_{ash}} \tag{8}$$

Here, H_C refers to the LHV of carbon. The variable x_{char} is the mass fraction of char on an ash-free basis, while the variables $x1_{char}$ and $x2_{ash}$ are the mass fractions of char and ash on a dry-fuel basis, respectively. Also h_C^o, h_{O2}^o, *and* h_{CO2}^o are the specific enthalpies of carbon, oxygen, and CO_2 [20], respectively, and M_{Ch}, M_{O2}, and M_{CO2} are the molecular weights of carbon, oxygen, and CO_2, respectively.

In like manner, the specific enthalpy of the bio-oil or bio-crude ($h_{C_aH_bO_d}^o$) which is collected as a liquid inside the flask after cooling the effluent gases and vapours, was estimated according to its heating value and elemental composition. The HHV of the bio-oil was adopted as 19 MJ/kg [21], which was later utilised to calculate the LHV of the bio-oil ($H_{C_aH_bO_d}$). Hence, the LHV was determined from the following correlation [22]:

$$H_{C_aH_bO_d} = HHV - 9H_{oil}(h_g) \tag{9}$$

where H_{oil} is the mass fraction of hydrogen in bio-oil [23], and h_g is the water enthalpy of vaporisation (kJ/kg).

The specific enthalpy of the bio-oil ($h^o_{C_aH_bO_d}$) was calculated according to the following equation [18]:

$$h_{C_aH_bO_d}^o = H_{C_aH_bO_d} + a\, M_{CO2} h_{CO2}^o + \frac{b}{2} M_{H_2O} h_{H_2O}^o - \left[a + \frac{b}{4} - \frac{d}{2}\right] M_{O2} h_{O2}^o \tag{10}$$

Here, $H_{C_aH_bO_d}$ is the LHV of the bio-oil. The variables a, b, and d are the atom number of carbon, hydrogen, and oxygen, respectively. Also $h_{H_2O}^o$ is the specific enthalpy of water [20].

The calculation of the specific enthalpy of tar followed the same procedure as in bio-oil, but with different hydrogen content, HHV value, and number of atoms representing the lumped chemical formula of the tar. Firstly, the HHV of the tar was adopted to be 25 MJ/kg, that is, the value for tar which accumulated on the cold walls of the cooling system [21]. Secondly, Eq. 9 was reapplied in order to compute the LHV, but with different hydrogen mass fraction [24]. Finally, the specific enthalpy of tar was calculated from Eq. 10, and the values for a, b, and d were specified according to the chemical formula of the tar. All the above-mentioned equations were employed in visual basic application (VBA) Excel spreadsheet to calculate the thermodynamic properties, which were considered part of the PEM.

2.1.4. Devolatilisation yield correlations

The yield of species (kg/kg EFB) from devolatilisation represents the first step in the model building, where successive reactions such as bio-oil, tar, methane conversion and WGSR take place in the FB of the reactor. In general, the yield of different products has been treated empirically from the experimental data against the temperature of the reactor. The scattered data were plotted in Excel spreadsheet, where add trendline function was used. As a result, seven correlations were obtained which regard to the yield of H_2, CO, CO_2, CH_4, bio-oil, tar, and char.

2.1.5. Kinetic and reactor model of secondary reactions conversion

The conversion of methane, bio-oil, and tar was kinetically modelled as first-order reaction, and a plug-flow reactor (PFR) model was assumed to represent the FB region of the reactor, since it has a tubular shape with a length of 46 cm. Under practical conditions, all the secondary reactions are kinetically limited, thus modelling them under equilibrium conditions provides inaccurate results [25]. In addition, the hydrocarbons adopted in this model to represent the bio-oil and tar are thermodynamically unstable under pure equilibrium models.

In fact, the generated methane from the primary decomposition of biomass is very resistant to secondary conversion unless a Ni-based catalyst is used at an adequately high temperature [25]. However, methane conversion is considered in this model because the methane was one of the main components released during devolatilisation of biomass, and its distribution compared to other species at different

temperatures is very important.

Equally important is modelling the liquid bio-oil as a separate component rather than lumping together with tar, which is deposited on the cold parts of the cooling system due to bio-oil yield variation at different conditions and its high energy density [26–28]. In the same way, the produced tar during devolatilisation was also modelled as an individual chemical compound so as to estimate roughly the tar yield and monitor the effects on the tar concentration while the pyrolyser operating conditions change. Moreover, tar has a high energy density in spite of its small yield, which may significantly affects the energy balance of the modelled system [25].

The conversion ($(conv)_i$) of the methane, bio-oil, and tar was calculated according to the equation below [29]:

$$(conv)_i = 1 - \exp(-Da_i)\ \mathrm{i} = \mathrm{CH_4}, \mathrm{bio-oil}, \mathrm{tar} \tag{11}$$

Here, Da is the Damköhler number, and can be expressed as below [29]:

$$Da_i = k_i \tau \tag{12}$$

where k_i is the rate constant of the individual species and τ is the residence time (s) of the produced gases in the FB.

The kinetic parameters of methane, bio-oil, and tar conversion are listed in Table 1. A pseudo-first order reaction was adopted for the methane kinetic equation, in which the rate constant is lumped with the concentration of water. As for tar, Jess (1996) [30] has suggested a first-order kinetic equation for homogenous thermal conversion of tar in excess of steam and hydrogen, represented by toluene, as shown in Table 1. In particular, the kinetic equation of tar decomposition is first order with respect to toluene concentration, while the steam and hydrogen concentrations orders are zero and 0.5, respectively. In this rate expression, the hydrogen concentration is lumped with the rate constant. The kinetic parameters concerning toluene conversion were estimated by means of a tubular flow reactor. The bio-oil decomposition was represented as a first order reaction for the homogenous gas phase reaction of the thermal decomposition of phenol.

Similarly, the WGSR is limited by kinetic factors, and the equilibrium is not achieved under actual gasification conditions [25]. However, this reaction was considered in this model, but kinetically modified by defining a factor (f_{WGSR}) described as below [4]:

$$f_{WGSR} = \frac{K_{exp}}{K_{WGSR}} \tag{13}$$

Here, the variable K_{exp} was estimated from the experimental data and can be expressed as follows:

$$K_{exp} = \left(\frac{y_{CO_2} y_{H_2}}{y_{CO} y_{H_2O}}\right)_{exp} \tag{14}$$

where y_i is the mole fractions of the gas species (CO_2, H_2, CO, and H_2O) released during experiment.

The K_{WGSR} was calculated from the equation listed in the Table 1.

2.1.6. Model's main equations

2.1.6.1. Atomic balance equations. The main structure of the model basically depends on the atomic balance of species that evolved from devolatilisation. In particular, the FB of the reactor, where the pyrolysis of EFB takes place, can be described by an overall atomic balance as written below:

$$\begin{aligned} &x_{C,EFB} + x_{H,EFB} + x_{S,EFB} + x_{O,EFB} + x_{N,EFB} + x_{H_2O,EFB} + w_{N_{2,ca}} \\ &= \left(\left(M_{H_2} y_{H_2}\right) + \left(M_{CO} y_{CO}\right) + \left(M_{CO_2} y_{CO_2}\right) + \left(M_{CH_4} y_{CH_4}\right) + \left(M_{H_2O} y_{H_2O}\right)\right. \\ &\quad \left. + \left(M_{N_2} y_{N_2}\right) + y_{bio-oil} + y_{tar}\right) \times F_{gp} + x_{char} \end{aligned} \tag{15}$$

The terms of Eq. 15 are in kg/kg EFB, where $x_{i,EFB}$ refers to the mass fractions of EFB constituents on dry basis. The variable $w_{N2,ca}$ represents the mass of nitrogen carrier gas required per 1 kg EFB (kg/kg EFB) into the system, while M_i and y_i are the molecular weight and mole fractions of the produced species, respectively.

The amount of ash remains constant during devolatilisation, so its term is cancelled out in Eq. 15. With regards to the calculations of pseudo-equilibrium gas composition, firstly, the unconverted amounts of methane, bio-oil, and tar were calculated from the equation written below, after estimating their conversion from kinetic rate expressions as explained and presented in Section 2.1.5 and Table 1.

$$Y_{i,gp} = Y_{i,dev.}\left(1 - (conv)_i\right)\ \mathrm{i} = \mathrm{CH_4}, \mathrm{bio-oil}, \mathrm{and tar} \tag{16}$$

Here, $Y_{i,gp}$ is the yield of CH_4, bio-oil, and tar deducted from the produced gas with the aim of achieving the equilibrium, the variable $Y_{i,dev.}$ is the yield of the previously mentioned components of devolatilisation, calculated from empirical equations of the experimental work in this research, and $(conv)_i$ is the conversion of the above three previous species.

Secondly, four atomic balance equations regarding the atoms (carbon, hydrogen, oxygen, and nitrogen) have been applied to estimate the pseudo-equilibrium composition, and can be written as follows:

$$\begin{aligned} &x_{C,EFB} - x_{char} - Y_{CH_4,gp}\frac{M_C}{M_{CH_4}} - 7Y_{tar,gp}\frac{M_C}{M_{tar}} - 6Y_{oil,gp}\frac{M_C}{M_{oil}} \\ &= \left(y_{CO} + y_{CO_2} + y_{CH_4}\right) M_C F_{gp} \end{aligned} \tag{17}$$

$$\begin{aligned} &x_{H,EFB} + 2\frac{M_H}{M_{H_2O}} x_{H_2O,EFB} - 4Y_{CH_4,gp}\frac{M_H}{M_{CH_4}} - 8Y_{tar,gp}\frac{M_H}{M_{tar}} - 6Y_{oil,gp}\frac{M_H}{M_{oil}} \\ &= \left(2y_{H_2} + 2y_{H_2O} + 4y_{CH_4}\right) M_H F_{gp} \end{aligned} \tag{18}$$

Table 1
Kinetics of gas phase reactions (methane reforming, toluene thermal decomposition, phenol thermal decomposition and water gas-shift reaction).

Reaction	Chemical equation	Reaction rate expression	Kinetic parameters	Ref.
Methane reforming	$CH_4 + H_2O \rightarrow CO + 3H_2$	$r_{CH_4} = kc_{CH_4} c_{H_2O}$(kmol m^{-3} s^{-1})	$k = k_0 e^{-E/RT}$ (1) $k_0 = 3.00 \times 10^8$ m^{3}kmol^{-1}s^{-1} E = 125 kJ mol^{-1}	[31]
Thermal decomposition of toluene	$C_7H_8 \rightarrow lighter\ \ compounds$	$r_{C_7H_8} = kc_{C_7H_8} c_{H_2}{}^{0.5}$(mol m^{-3} s^{-1})	$k = k_0 e^{-E/RT}$ (2) $k_0 = 3.3 \times 10^{10}$ m$^{1.5}$ mol s^{-1} E = 247 kJ mol^{-1}	[30]
Phenol decomposition	$C_6H_6O \rightarrow diff.\ \ compounds$	NA	$k = k_0 e^{-E/RT}$ (3) $k_0 = 1.00 \times 10^{12}$ s^{-1} E = 254 kJ mol^{-1}	[32]
Water gas-shift reaction	$CO + H_2O \underset{ki}{\overset{kd}{\rightleftharpoons}} CO_2 + H_2$	$r_{CO} = k_i(c_{CO_2} c_{H2} - K_{WGSR} c_{CO} c_{H_{2O}})$ (kmol m^{-3} s^{-1})	$k_i = k_0 e^{-E/RT}$ $k_0 = 1.41 \times 10^5$m^{3}kmol^{-1} s^{-1} E = 54.2 kJ mol^{-1} $K_{WGSR} = 0.029\exp\left(\frac{4094}{T}\right)$ (4)	[33]

NA: Not applicable

$$x_{O,EFB} + \frac{M_O}{M_{H_2O}} x_{H_2O,EFB} - Y_{oil,gp}\frac{M_O}{M_{oil}} = \left(y_{CO} + 2y_{CO_2} + y_{H_2O}\right) M_O F_{gp} \quad (19)$$

$$x_{N,EFB} + w_{N_2,ca} = y_{N_2} M_{N_2} F_{gp} \quad (20)$$

The equilibrium expressions for the steam reforming of methane (SRMR) and WGSR are considered together in Eqs. 17–20, which can be written as follows [25]:

$$\frac{y_{H_2} y_{CO_2}}{y_{H_2O} y_{CO}} = f_{WGSR}\left(0.029 exp\left(\frac{4094}{T}\right)\right) \quad (21)$$

$$\frac{y_{H_2}^3 y_{CO}}{y_{CH_4} y_{H_2O}} = \left(6.14 \times 10^{13} exp\left(\frac{-28116}{T}\right)\right) \quad (22)$$

where the terms inside the brackets of Eqs. 21 and 22 refer to the equilibrium constants of WGSR and SRMR, respectively.

2.1.6.2. Overall heat balance equation. The overall heat balance equation is used to model the FB section of the reactor where pseudo-equilibrium of the released gases from devolatilisation are supposed to occur. In particular, this equation implies the enthalpy of the formation of EFB, the specific enthalpy of the accompanied water, and specific enthalpy and heat capacity of carrier gas nitrogen. The energy of the product stream consists of the specific enthalpies and heat capacities for both the produced gases and char. The enthalpy equation can be expressed as below:

$$h_{f,EFB}^{o} + x_{H_2O,EFB} h_{f,H_2O} + w_{N_2,ca} h_{f,N_2} + w_{N_2,ca} \int_{T_0}^{T_i} C_{p,N_2} dT = F_{gp} \sum_{i=1}^{8} y_i h_{f,gp,i} + F_{gp} \sum_{i=1}^{8} y_i \int_{T_0}^{T_{FB}} C_{p,gp,i} dT + x_{char} h_{f,C} + x_{char} \int_{T_0}^{T_{FB}} C_{p,char} \quad (23)$$

2.1.7. Model solution procedure

The solution procedure of the PEM was carried out by writing a code in VBA Excel spreadsheet. The method of the solution comprises many steps as written below:

1 Model main inputs:
   - fuel characteristics: includes the ultimate and proximate analysis of the EFB and its molecular weight;
   - reactor dimensions: includes the inner diameter of the reactor, and the height of the FB;
   - gas flow rate and temperature: this is about supply flow rate of the nitrogen carrier gas, and its inlet temperature;
   - heat of vaporisation for water, pressure inside the reactor, and universal gas constants are additional inputs to meet the requirements of the solution.
2 One of the numerical solution requirements is the relaxation factor for updating the old values of the variables in step 3.
3 The composition and the flow rate of the produced gases, and the temperature of the FB are supplied to the model as initial guess to start the procedure of the solution.
4 Estimation of the thermodynamic properties of all species by interpolation in order to be used later in the model.
5 Feeding the model with the empirical correlations of the produced components during devolatilization experiment.
6 Calculations of methane, bio-oil, and tar conversion by applying the kinetic equations listed in Table 1. In addition, the approaching equilibrium factor for WGSR is also estimated.
7 Determine the amount of unconverted methane, bio-oil, and tar from Eq. 16 to be subtracted from the pseudo-equilibrium equations.
8 Solve the Eqs. 17–22 for predicting the pseudo composition of the gases, by presenting them in the Jacobian matrix form and be solved according to the Newton-Raphson method as written below [34]:

$$(val)_{n+1} = (val)_n - J_F^{-1}(x_n) F(x_n) \quad (24)$$

where the variable $J_F^{-1}(x_n)$ refers to the inverse of Jacobian matrix, $F(x_n)$ is the vector of the initial values, whereas $(val)_{n+1}$ and $(val)_n$ represent the new and old values, respectively.

1 Solve for the overall atomic and heat balance equations for estimating the total produced gas flow and the temperature of the FB.
2 Finally, updating the estimated values from the model, and repeat the procedure iteratively in step 2 by replacing the initially assumed values with the new predicted. The iteration stops when the convergence is achieved.

2.1.8. Sensitivity analysis of devolatilisation

A sensitivity study was carried out on the devolatilisation sub-model of the EFB to investigate the influence of the main parameters on the tar and remaining products of this process. Amongst these parameters, the sweep or carrier gas nitrogen flowrate was varied from 10 to 30 L/min in an increment of 5 L/min. In addition, the temperature of the reactor was tested between 650 to 850 °C with a step size of 25 °C since the experimental work of the pyrolysis took place at isothermal conditions.

2.2. Experimental devolatilisation of empty fruit bunches (EFB)

Three devolatilisation experiments were performed at different pyrolysis temperatures to predict the behaviour of the EFB thermal decomposition. In each experiment run, the temperature was fixed at constant values for the purpose of kinetic study. High temperatures were favoured for this kind of experiment rather than temperatures of 500 ℃ and below since the purpose of the research is to predict gas composition from gasification. So, the first stage of gasification, the devolatilisation reactions, are to be considered at 650, 750, and 850 ℃. On the other hand, other parameters such as particle size and nitrogen flowrate were kept constant at 15 L/min.

2.2.1. Fluidised bed pyrolyser

The thermal decomposition (or devolatilisation) of EFB was investigated in a bench scale fluidised-bed reactor. The reactor is made of stainless steel (type 316), cylindrical, 600 mm in length with outer and inner diameter of 43 mm and 40 mm, respectively. The first part of the reactor is the furnace, which consists of a large chamber of a split type. This type of chamber enables the furnace to be opened from one side for dismantling and cleaning purposes. Three type-K thermocouples are available for a heating system: at the centre (300 mm from the upper flange), upper (50 mm below the upper flange), and at the bottom of the reactor (50 mm above the bottom flange). A batch of biomass was fed from a feeding point at the top. In the devolatilisation experiments, nitrogen was used instead of gasifying agents in order to provide an inert environment necessary for the thermal decomposition of the EFB. The nitrogen was supplied from a cylinder controlled by a nitrogen flowmeter, which eventually flowed into the reactor through a cone-shaped perforated plate that contains 50 holes (ID = 1 mm) located at the bottom of the reactor. The bench-scale reactor is shown in Fig. 3 and described in Table 2.

2.2.2. Experimental setup

In this research, an experimental setup was established for kinetic study of the EFB devolatilisation reaction. The devolatilisation of EFB was conducted in a fluidised-bed reactor. The EFB feeding was carried out via a three-quarter inch (19 mm) stainless steel tube with a valve

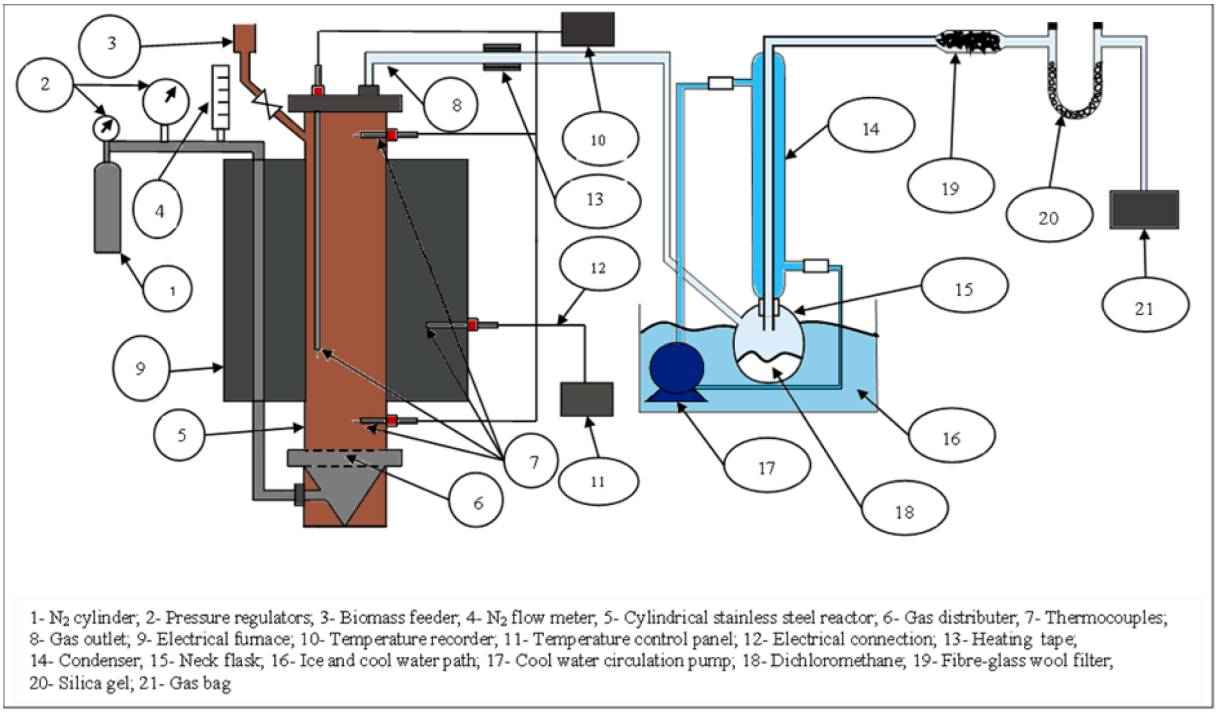

Fig. 3. A schematic diagram of the lab-scale fluidised-bed gasifier.

Table 2
The dimensions of the lab-scale fluidised-bed gasifier and its parts.

Part Name	Diameter (mm)	Length (mm)
Reactor	40	600
Furnace	60	450
Flange (upper & bottom)	90	10
Air distributor	35	5
Air inlet	3.1	650
Gas outlet	12.7	300
Feeder	19	150

located at the top part of the reactor. Nitrogen was used to provide an inert environment and was supplied from a cylinder connected to a nitrogen flow metre to obtain the required flow rate. The nitrogen passed through the reactor from the base of the pyrolyser by means of a stainless-steel nozzle under the nitrogen distributor plate. The produced gas left the top of the reactor via half inch (12.7 mm) stainless steel tubing.

The tubing was kept at 250 ±5 °C by using a heating tape to prevent condensation of tar vapour in the produced gas and to reduce blockage issues in the outlet tube. The produced gases passed into the cooling system, consisting of one neck flask (1000 mL) immersed in a circulating cooling box filled with ice and a condenser (50 cm height). The neck flask contained 100 mL of dichloromethane (DCM) to collect the condensed vapours of bio-oil from the produced gas. The non-condensable gas left the cooling system and passed through a filter of fibre-glass wool to trap more tar. Another type of filter used in this experiment is silica gel filter to dry the gas from the wool filter. The gas was collected using 10 L gas bags (SKC, USA) for characterisation and analysis. The configuration of the devolatilisation experimental setup is shown in Fig. 3.

2.2.3. Thermal decomposition behaviour and kinetic analysis

A series of isothermal experiments were carried out in a lab-scale fluidised-bed reactor, as shown previously in Fig. 3. The dried EFB was top fed into the reactor as a batch of approximately 10 g after reaching the steady temperature inside the reaction zone. The effluent dried gases from the reactor system were collected every 15 s using 10-litre gas bags.

A reaction model for volatiles release was applied to calculate the kinetic parameters. In this model, the rate of the reaction shows dependence on the mass of the volatiles and temperature. The rate equation can be presented as follows [35]:

$$\frac{dW_{EFB}}{dt} = -k \,.\, W_{vol}(t)^{n^*} \tag{1}$$

where W_{EFB} is the mass of EFB and k is the rate constant (s^{-1}), whereas n* refers to the reaction order.

The Arrhenius equation was introduced to the calculations to estimate the kinetic parameters of the devolatilisation. The equation is presented below:

$$k = k_0 \exp\left(-\frac{E}{RT}\right) \tag{2}$$

where k_0 is the pre-exponential factor (s^{-1}), E is the activation energy (kJ/mol). R represents the gas constant (0.008314 kJ/mol. K), and T is the absolute temperature (K).

3. Results and discussion

3.1. Experimental correlations

From the pyrolysis data, empirical correlations were established relating the yield of the evolved gas species (H_2, CO, CO_2 and CH_4), the produced bio-oil, tar and char to the final pyrolysis temperature. These yield correlations were based on the amounts of the products measured in grams per the amount of the fuel or EFB measured in grams (g/g_{fuel}), as listed in Table 3. The linear model was chosen to fit the experimental data for gases and tar through applying the linear regression model which minimised the squares of difference between the observed (experimental) and predicted data. Particularly, this model was applied since the relationship between the yield of pyrolysis products and temperature appeared to be linear [36,37].

Table 3
Yield correlations of pyrolysis products.

Species name	Correlations	R^2	$\|\|e\|\|$	RMSE
H_2	$Y = 7 \times 10^{-6}T - 0.0031$	0.63	0.000787	0.000787
CO	$Y = 4 \times 10^{-5}T + 0.0114$	0.09	0.018137	0.018137
CH_4	$Y = 9 \times 10^{-5}T - 0.0584$	0.80	0.006751	0.006751
CO_2	$Y = -0.0009T + 0.8277$	0.85	0.054622	0.054622
Bio-oil	$Y = 3 \times 10^{-6}T^2 - 0.0041T + 1.9514$	Na	Na	Na
Char	$Y = 5 \times 10^{-6}T^2 - 0.0078T + 3.2125$	Na	Na	Na
Tar	$Y = -8 \times 10^{-5}T + 0.0808$	0.87	0.004311	0.004311

Na: not applicable.

3.2. Kinetic analysis of EFB pyrolysis

The kinetic parameters of EFB thermal decomposition were compared with literature. Generally, the value of E widely varies depending on the reactor type (fluidised bed, screen heaters, drop tubes and thermogravimetry), sample size and type of biomass, and the manipulation of experimental data (or type of mathematical model applied). In particular, this value comprises two ranges (56 –174 kJ/mol) for the primary decomposition at low and high temperatures, whereas (66 – 123 kJ/mol) was for the secondary reactions at high temperatures [13]. In this research, the estimated value of E was 109 kJ/mol which belonged to the latter range. This value indicated well agreement with literature that consider the secondary reactions, especially the cracking of tar vapours. The values of k_0 and E were in the same region of high temperatures where the secondary reactions took place, as shown in Table 4. However, the occurrence of the primary decomposition reactions might also overlap with the secondary reactions.

3.3. Chemical formula and equation of EFB

The resulted chemical formula of EFB is $CH_{1.67}O_{0.74}$ which was determined from ultimate analysis of EFB on dry basis. This formula was used in estimation of stoichiometric coefficients of the EFB thermal decomposition through CRS approach because of the complexities of the pyrolysis mechanism, the absence of individual chemical reactions, and the occurrence of many heterogeneous and homogeneous reactions simultaneously. As a result, the decomposition of EFB was represented by a single balanced chemical equation to describe the whole process of pyrolysis, as written in Eq. 25.

$$CH_{1.67}\ O_{0.74} \rightarrow 0.61833\ H_2 + 0.65333\ CO + 0.021667\ CO_2 + 0.021667\ CH_4 + 0.021667\ H_2O + 0.021667\ C_6H_5OH + 0.021667\ C_7H_8 + 0.021667\ C \quad (25)$$

3.4. Model predictions comparison with experimental work

The outputs of the developed model were compared with the experimental work carried out in a bubbling fluidised bed reactor with N_2 as the carrier gas. The main inputs of the models were as follows: the initial estimates of the species mole fractions of H_2, CO, CO_2, CH_4, N_2, and H_2O - expressed as y_1, y_2, y_3, y_4, y_5, and y_{10}, respectively. Another main input parameters were required to run the model, as presented in Table 5. The flow of N_2 (F_{N2}) and its temperature (T_i) were amongst the inputs required to run the model. Particularly, the same conditions of the experiments were applied as the model inputs. The temperature of pyrolysis (T_p) was assumed to be the same of T_i since the external heating source was not considered, so the required heating for EFB decomposition was achieved through the hot N_2 flow.

Table 4
Kinetic parameters of EFB devolatilisation.

k_0 (s^{-1})	E (kJ/mol)	References
9.595E+03	109	This study
4.28E+06	107.5	[38]
4.5E+06	110.1	[39]
1.13E+03	109	[40]

Table 5
Pyrolysis model input parameters.

Model inputs	Assigned value
Proximate analysis (wt. fraction):	
Moisture wet basis	0.556
Moisture dry basis	0.0518
Ash	0.0345
Ultimate analysis (wt. fraction, db):	
C	0.4662
H	0.0645
S	0.00035
O	0.4566
N	0.0121
Latent heat of steam (hg, kJ/kg)	2260
Pressure (P, atm)	1
Universal gas constants:	
R (m^3 atm K^{-1} mol^{-1})	8.206×10^{-5}
R2 (kJ K^{-1} mol^{-1})	8.314×10^{-3}
EFB molecular weight (kg/kgmol)	25.35
Reactor geometry:	
Inside diameter (m)	0.04
Height (m)	0.6
Relaxation factor	0.002

db - dry basis

The predicted gas composition from PEM and experimental results are listed in Table 6.

Generally, the model fair predicted the output gas composition. The yields of tar, bio-oil, char, and methane at the outlet of the reactor were compared with equilibrium model (EM). The tar prediction from PEM indicated a good agreement with experimental data with RMS of 0.003. Similarly, the predicted conversion of the tar is about 59.7% while that from the experiments is around 51.5% (at 850 °C and 0.24 s residence time), as shown in Table 7.

The model exhibited a slightly higher conversion due to use of an ideal plug-flow reactor model (PFR) to represent the conversion of the tar in the freeboard (FB) of the reactor. In fact, the PFR assumes perfect mixing in the radial direction. As reported by Gomez-Barea and Leckner [4], the gas velocity is high in the axial direction and consequently convection dominates the transport mechanism rather than radial distribution of gases. In other words, poor gas mixing occurs in the radial direction which results in a gradient in the gas concentration. This gradient is also obtained from non-uniform distribution of biomass, as reported in [41]. This is likely the case which takes place in top feeding reactors, where the devolatilisation occurs in the long FB and maldistribution of gas occurred. In fact, the gas mixing decreases considerably when ascending to the FB [42]. However, modelling the FB using PFR is a good representation for gas motion which gives reasonable predictions, as reported in [43]. Meanwhile, the reported tar conversion for birch wood pyrolysis in a fluidised-bed reactor was approximately 60% at 850 °C (2 s residence time) [44]. In addition, Morf [45] reported the conversion of sweet gum hardwood in two-chamber reactors which ranged between 9 and 88% at temperatures of 500 and 800 °C (and residence time 1 s), respectively.

As shown in Table 6, the highest deviation obtained in the yield of CH_4 and CO where the RMS was 2.840 and 6.049, respectively. This is because a correction for the equilibrium reaction of methane steam reforming (SRMR, Eq. 22) was not employed in the model, but PFR model was applied to consider the conversion of CH_4. The backward path for this reaction is endothermic which is favoured at high temperatures forming more CO. However, applying the kinetic approach on this reaction corrected the consumption of the CH_4 where almost

Table 6
Comparison between PEM prediction and experimental results.

Run	1		2		3		RMS
	Experiment	PEM	Experiment	PEM	Experiment	PEM	
Temperature (°C)	650	650	750	750	850	850	
Output gas (mol%, moisture free)							
H_2	0.394	1.845	0.319	1.113	0.283	0.600	0.972
CO	0.964	3.286	0.206	5.988	0.389	8.814	6.049
CO_2	3.381	2.366	0.436	2.016	1.043	0.810	1.092
CH_4	0.221	2.745	0.095	3.344	0.458	3.157	2.840
N_2	95.041	89.758	98.944	87.540	97.827	86.618	9.722
Yield of bio-oil, tar, and char (g/g EFB)							
Bio-oil	0.38	0.595	0.337	0.194	0.327	0.121	0.190
Tar	0.0309	0.031	0.018	0.023	0.015	0.013	0.003
Char	0.203	0.255	0.100	0.175	0.093	0.195	0.079

Table 7
Comparison of tar conversion between PEM prediction and experimental measurement.

Component	Conversion
Tar predicted from PEM	59.7%
Tar from experiments	51.5%

constant consumption rate was obtained. As reported by Gomez-Barea and Leckner [25], low rate was observed for SRMR below 1000 °C due to less interaction in secondary reactions which hardly affected without using Ni-based catalyst. Moreover, it is more likely that the produced CH_4 from the experiments is low due to incomplete tar conversion because of low residence time (0.24 s), where CH_4 is one of the main products produced from tar cracking reactions [46]. However, as reported in [47], the yield of CH_4 was not predicted and CO was overestimated for sawdust gasification using normal equilibrium model at 832 °C.

Meanwhile, Karamarkovic and Karamarkovic [48] validated their results for gasification model against the experimental results of Altafini et al. [47] at 832 °C. In their work, two cases for carbon conversion were considered: 92 and 100%. The former case employed an assumption for the unreacted char which was 8%. Underprediction of CH_4 yield was reported in both cases despite applying the correction factor for WGSR and SRMR. Jarungthammachote and Dutta [11] presented two equilibrium models for gasification at 800 °C: normal equilibrium model and modified equilibrium model. In the first model, the yield of CH_4 was underestimated, while this value increased in the modified model. In the modified model, the authors adopted two correction factors for WGSR and CH_4 formation reaction (char-H_2 reaction). These factors were calculated based on the average ratio of CO and CH_4 produced from eleven experiments reported in literature to correct the equilibrium deviation of WGSR and CH_4 formation.

The predictions of H_2 as reported in Table 6 are higher than experimental measurement, especially at low temperature (650 °C), which later the predictions decreased and almost approached the experimental value at 850 °C. This observation is due to the effects of the previously discussed reaction (SRMR), which produced high yield of CO. As a result, higher H_2 yield was obtained in WGSR at low temperature through consuming the produced CO. As reported by Basu [12], the maximum yield of H_2 resulted from WGSR at low temperatures since the forward path is exothermic. Karamarkovic and Karamarkovic [48] also reported overestimation in the predictions of H_2 at 100% conversion, and observed that the yield of H_2 decreased when a constant char yield was adopted, which corresponds to about 92% conversion of char. An overestimation in the yield of H_2 was also reported by Altafini et al. [47]. Meanwhile, Jarungthammachote and Dutta [11] observed a decrease in H_2 yield from the modified model compared to normal equilibrium model.

As seen in Table 6, the yield of CO_2 is well predicted with RMS of 1.092 when validated against the experimental work. As reported by Altafini et al. [47], normal equilibrium model underestimated the yield of CO_2. Jarungthammachote and Dutta [11] reported a CO_2 underestimation for from unmodified model (normal equilibrium), while this value increased in their modified model. Karamarkovic and Karamarkovic [48] slightly improved the yield of CO_2 when constant yield of char was assumed. The yield of N_2 is fairly predicted with RMS of 9.722. Karamarkovic and Karamarkovic [48] underestimated the yield of N_2 at 100% conversion, but an increase was noticed on this value when char yield was fixed at the outlet of the gasifier. Meanwhile, the yield of the bio-oil and char revealed good prediction with RMS of 0.190 and 0.079, respectively.

Unlike PEM, the normal and modified equilibrium models could not predict the yield of tar and bio-oil since their hydrocarbon content is thermodynamically unstable [49]. In some cases, the former model is not capable to predict or underestimates the yield of CH_4 [50]. Moreover, some modified models underestimate the yield of CH_4 despite applying a correction to the SRMR. Both normal and modified equilibrium models are not capable to prove the stability of SRMR at temperatures below 1000 °C, whereas the PEM highlights the insignificance of methane conversion at these temperatures. In the modified models, the corrections are applied to WGSR and SRMR, which are calculated according to the yield of CO and CH_4 produced in different systems. However, the correction of WGSR in the PEM is calculated internally in the model. Meanwhile, the char yield is not predictable in both models. Hence, some modified models adopt the value of the remaining char from literature to correct the individual gas species yield.

The PEM also highlights on the kinetic limitations of WGSR under the experimental conditions (this study) rather than reaching equilibrium. In fact, the correction factor for the equilibrium deviation (f_{WGSR}, Eq. 13) was calculated in the PEM, which equals to the ratio of the experimental (K_{exp}, Eq. 14) to the theoretical (K_{WGSR}, Table 1) equilibrium constants. This factor has a value ranging between 0.1 and 0.07 at temperatures between 650 and 850 °C. The equilibrium constant of WGSR decreases when the temperature increases [12]. The ratio of less than 1 shows that WGSR has never reached equilibrium in the experimental work (this study) at 650 – 850 °C.

The predictions of K_{exp} should be below or approaching the K_{WGSR} predictions [51], as shown in Fig. 4. K_{exp} and K_{WGSR} from this study were compared with the study reported in [52] where a comparison with JANAF tables is available. A comparison was also made for WGSR equilibrium constant with predicted data reported by Gao and Li [52]. In their study, the pyrolysis zone of a downdraft gasifier was modelled at a heating rate of 25 K/min and 1400 K. Their work predicted high value of equilibrium constant at low temperature (627 °C), as shown in Fig. 4. It is likely because of the high concentration of CO_2 produced in the combustion reactions, where the combustion and devolatilisation were assumed to take place simultaneously. Moreover, Gao and Li assumed complete combustion of char. Thus, high yield of CO_2 obtained which eventually resulted in high equilibrium constant.

According to Yan et al. [51], the value of theoretical constant mainly

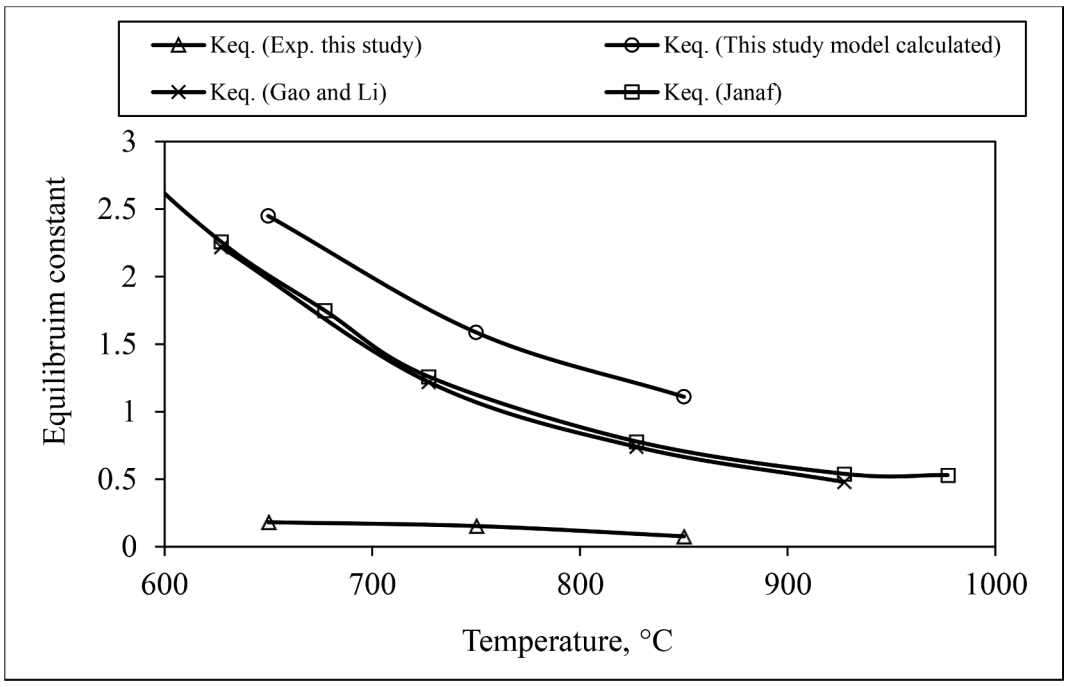

Fig. 4. Comparison of experimental (this study) and model (this study), predicted equilibrium constant of WGSR with JANAF tables and Gao and Li (2008) [52].

depends on concentration of CO_2 and H_2. Moreover, the equilibrium constant from JANAF is calculated theoretically from the calculation of Gibbs free energy for WGSR reaction. In this study, the devolatilisation zone was decoupled from combustion zone because of high rates of devolatilisation compared to combustion (char-O_2). Particularly, the diffusion of gasifying agent into char particles is slow due to diffusion resistance. However, the trends of K_{exp} and K_{WGSR} (this study) show the same decreasing trend of that reported in Gao and Li's study (2008).

The distribution of total carbon between gas phase and the remaining char was calculated for both experimental work and PEM at 850 °C using one kg of EFB as a basis, as depicted in Fig. 5. The model predicted 0.304 kg of carbon in the gas phase. Meanwhile, the calculated value from the experimental work was 0.303 kg. From the proximate analysis of EFB, the estimated carbon release into the gas phase was 0.3765 kg. This value was calculated by the difference between total carbon and fixed carbon (FC) of the original EFB, which were adapted from the ultimate and proximate analyses, respectively. The missing mass of carbon in both cases (experiment and model) was due to lumped chemical formula of bio-oil and tar. Moreover, the light gases (C_2 to C_6) were not measured and represented in the experiment and model. The remaining char composition was totally assumed as a pure carbon. Thus, the predicted carbon in the solid phase was 0.195 kg, while that from experiment was

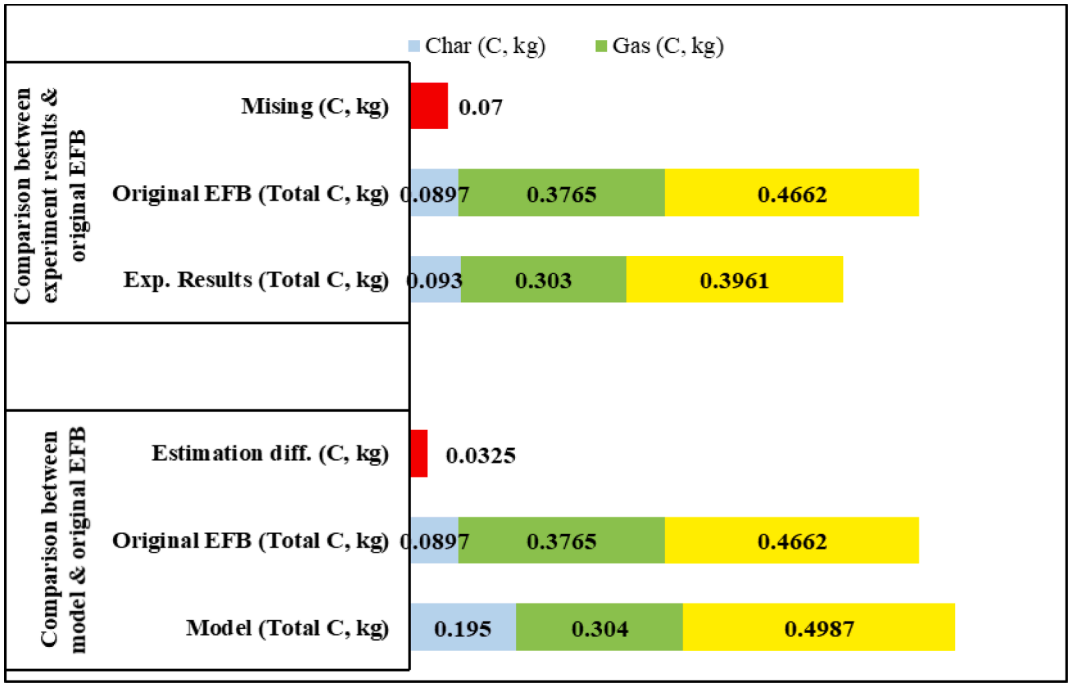

Fig. 5. Comparison of original EFB carbon content with experimental results and PEM predictions.

0.093 kg. This experimental value was consistent with the FC of EFB (0.0897 kg). Overall, the PEM predictions were reasonably well when compared with the experiment and analysis of EFB.

In addition, the distribution of carbon amongst gas species was compared between experimental measurement and PEM prediction under same conditions discussed previously, presented in Fig. 6. The PEM predicted that 39% of the initial carbon was transferred to CO, followed by 22% and 14% for biocrude and methane, respectively. Meanwhile, the lowest share of carbon was 3% which belonged to CO_2 and tar. The high share of carbon was for CO due to lack of correction for SRMR. As a result, more CO formed at high temperatures through enhancing the forward path of this reversible reaction. Meanwhile, the predicted carbon content in the biocrude is less than the experimental measurement due to the use of PFR model to represent the conversion of biocrude where high conversion around 79% obtained, compared to that from experiments (14%). The remaining percentage was 19% representing the difference between the EFB carbon content and predicted carbon in the gas phase. The difference was due to considering permanent gas species only such as CO, CO_2, and CH_4, while other hydrocarbon gases were neglected. Liquid oil and tar were modelled as phenol and toluene, respectively.

The experimental work indicated that 67% of the initial carbon was converted into the bio-oil which corresponds to 32.7 wt% oil, as illustrated in Fig. 6b. This value is in good agreement with the findings reported in [53], where the yield of liquid for different biomass wastes ranged between 17 to 43 wt % at temperatures between 600 and 900 °C.

Furthermore, Abdullah and Gerhauser [21] reported high carbon content in the bio-oil derived from EFB at 500 °C, which reached about 83 wt % for both organic and aqueous phases. On the other hand, only 6% of carbon was found in CO_2 followed by 4% in tar, whereas CO and CH_4 carbon share was 2%. The carbon content in CO_2 is higher than CO because of high ratio of CO_2 compared to CO with the highest value of 3.5 at 650 °C and decreased to 2.5 at 850 °C. The findings are consistent with other studies that reported that main gases from pyrolysis of biomass at low temperature are CO_2 followed by CO [53,54]. Moreover, WGSR which is thermodynamically favoured at low temperature affects the gas composition [12]. The conversion of CO increases towards forming more CO_2 and H_2 at low temperature. The yield of (CO_2 and H_2) tends to decrease at high temperatures because this reaction is kinetically favoured. Meanwhile, the gas residence time is another key factor affecting WGSR. In fact, H_2 in the bulk gas is mainly produced from the tar conversion [45]. In particular, low tar conversion at short residence time means less H_2 produced and consequently low yield of CO. As a result, low equilibrium constant is obtained for WGSR and consequently low f_{WGSR}. The high yield of CO_2 was due to high oxygen content of EFB, where high rate of CO_2 evolution was noticed by during pyrolysis of EFB at temperatures 200 – 500 °C [55]. Therefore, the initially formed CO_2 during primary decomposition of EFB at low thermal conditions (~ 500 °C) might not consumed into large extent through gas phase secondary reactions. For the same reason stated above regarding model part, the hydrocarbon gases (C_2 – C_6) were not measured during experimental work; consequently, the percentage of not detected carbon was 19%.

3.4.1. *Effect of temperature on pyrolysis yield*

The first reason behind adopting this type of model (PEM) was because of the significance of devolatilisation which reduced about 80 wt% of the total biomass weight. As a result, complex interaction amongst the primary released products took place affecting their degree of conversion which led to secondary path of reactions. Second, many of the reported literature about equilibrium models were incapable to

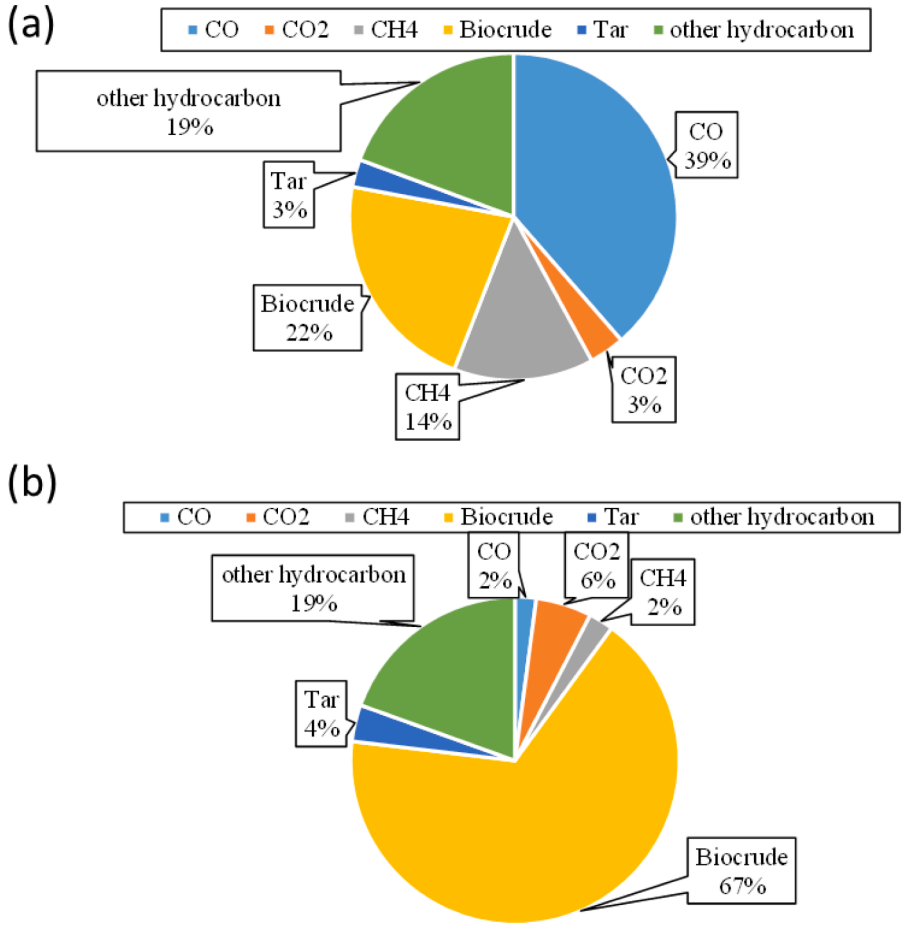

Fig. 6. Distribution of carbon in the gas phase (a) PEM prediction (b) experimental work.

predict the yield of liquid biocrude and tar.

Furthermore, the uncertainty increased due to adjustment of tar and methane conversion as well as the ratio of experimental to theoretical equilibrium constant for water-gas shift reaction (f_{WGSR}). Thus, the carbon transferred into the gaseous phase resulted in over and under predictions of gaseous products and with no information on char quantity. As shown in Fig. 7a, the predicted H_2 decreased from around 20 to 5 mol% as the temperature increased from 650 to 850 °C due to the representation of WGSR in the model, where increasing temperature enhances the backward reaction to consume more H_2 and CO_2. In contrast, the experimental measurement indicated an increment from 7 to 30 mol% as the temperature increased from 650 to 750 °C, confirming cracking reactions. The H_2 composition subsequently reduced to 13 mol % as the temperature increased to 850 °C. The predictions well agreed with the experimental data between 750 to 850 °C indicating the domination of water-gas shift reaction (WGSR).

As can be seen in Fig. 7b, the predicted concentration of CO doubled as the temperature increased from 650 to 850 °C. Meanwhile, experimental measurement showed that the concentration increased by 22% at 750 °C, and then went down slightly by 11% at 850 °C. Meanwhile, the model indicated an almost steady trend for CH_4 where the composition is stable at temperature below 1000 °C, whereas rose gradually in the experimental work due to cracking reactions of light hydrocarbons and tar, as depicted in Fig. 7c. The predicted CO_2 composition demonstrated a declining trend where 73% reduction was recorded as the temperature increased from 650 to 850 °C. The experimental data dropped from 71% to 40% for temperature range of 650 to 750 °C, and then slowly rose to almost 48% at 850 °C, as illustrated in Fig. 7d.

As shown in Fig. 8a, the model predicted 0.6 g/g EFB yield of biocrude at 650 °C where the value declined considerably to 0.12 g/g EFB at 850 °C. Experimental data exhibited a slight decrease from 0.38 to 0.33 g/g EFB within the same temperature range. Fig. 8b depicted model prediction and experimental measurement of tar yield where both curves demonstrated a decreasing trend with good agreement. Char yield is presented in Fig. 8c. The predicted char yield decreased from 0.26 to 0.20 g/g EFB while experimental work recorded a drop down to 0.09 g/g EFB as temperature increased. The findings are in good agreement with [56,53].

Fig. 9a presented the conversion of EFB from both model and experimental work where an increasing trend to 0.81 and 0.91, respectively was observed. In Fig. 9b, the total gas yield predicted from the model increased from 0.22 to 0.28 Nm^3/kg. Similarly, the trend from experimental measurement increased from 0.22 to 0.29 Nm^3/kg.

To sum up, the model fairly predicted the changes in gas composition with temperature variation. In particular, the backward reaction of WGSR was driven toward consuming H_2 and CO_2 to produce more CO with significant effect on H_2 yield. Furthermore, the equilibrium of WGSR was never reached due to its kinetic limitation. The domination of WGSR in gas phase reactions was clear in the model predictions and experimental results. In fact, the experimental data presented lower extent of cracking reactions than WGSR, particularly at temperatures higher than 750 °C. This behaviour was caused by the availability of CO_2 in the system in comparison to the yield of tar. The high ratio of CO_2/tar consumes more H_2 through WGSR [57]. Correspondingly, the model well predicted the unconverted carbon which transferred into the solid phase as char. The trend of the predicted char fairly agreed with that produced during experiments. According to Gomez-Barea and Leckner [25], the conversion of char was an important parameter affecting the performance of the fluidised-bed gasifier. Moreover, the predicted conversion of EFB indicated a good agreement with the experimental work of this study and literature. Dupont et al. [58] reported that the conversion of biomass ranged between 78 to 87% for temperatures from 800 to 1000 °C. Finally, the predictions and trends of liquid biocrude and tar to temperature change is illustrated in Fig. 10. The root mean squares (RMS) for biocrude and tar yields were 0.194 and 0.003, respectively.

3.4.2. *Effect of carrier gas flow rate on pyrolysis yield*

The effects of carrier gas flow rate on devolatilisation yield of EFB were investigated by changing the flow rate of N_2 from 10 to 30 L/min

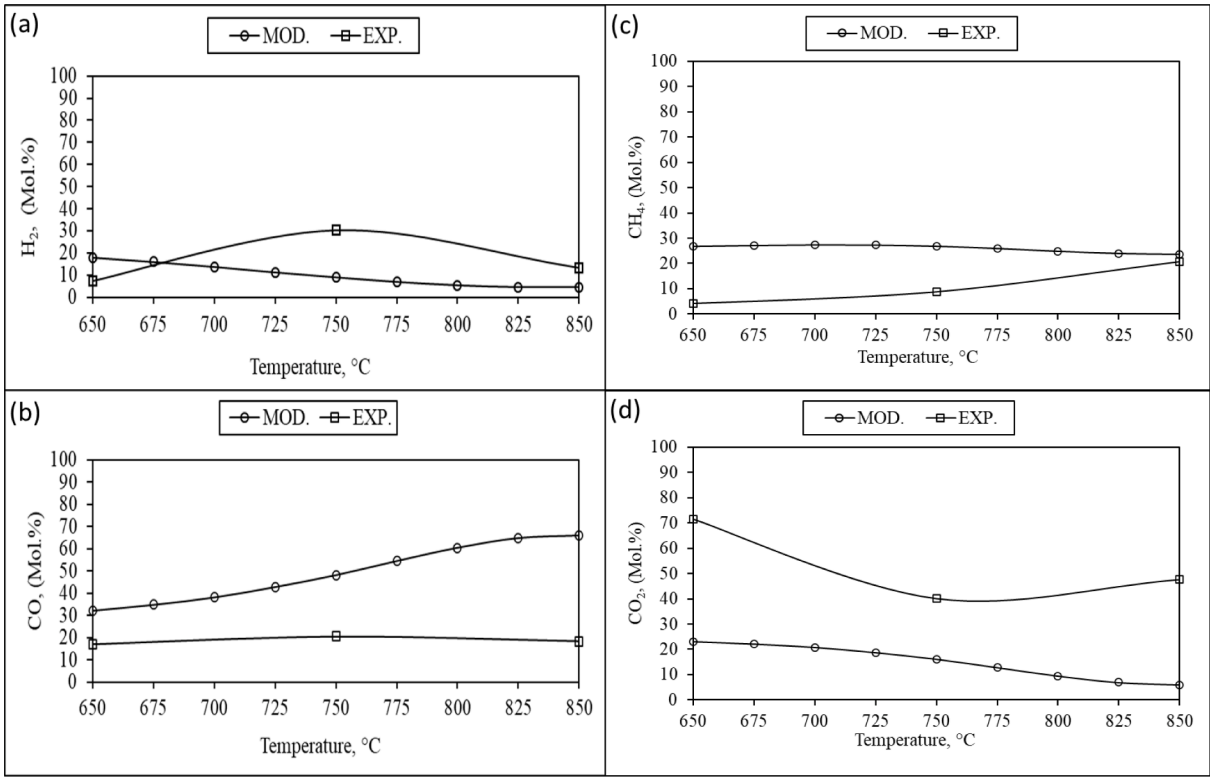

Fig. 7. Experimental measurement and model prediction (a) H_2, (b) CO, (c) CH_4, (d) CO_2.

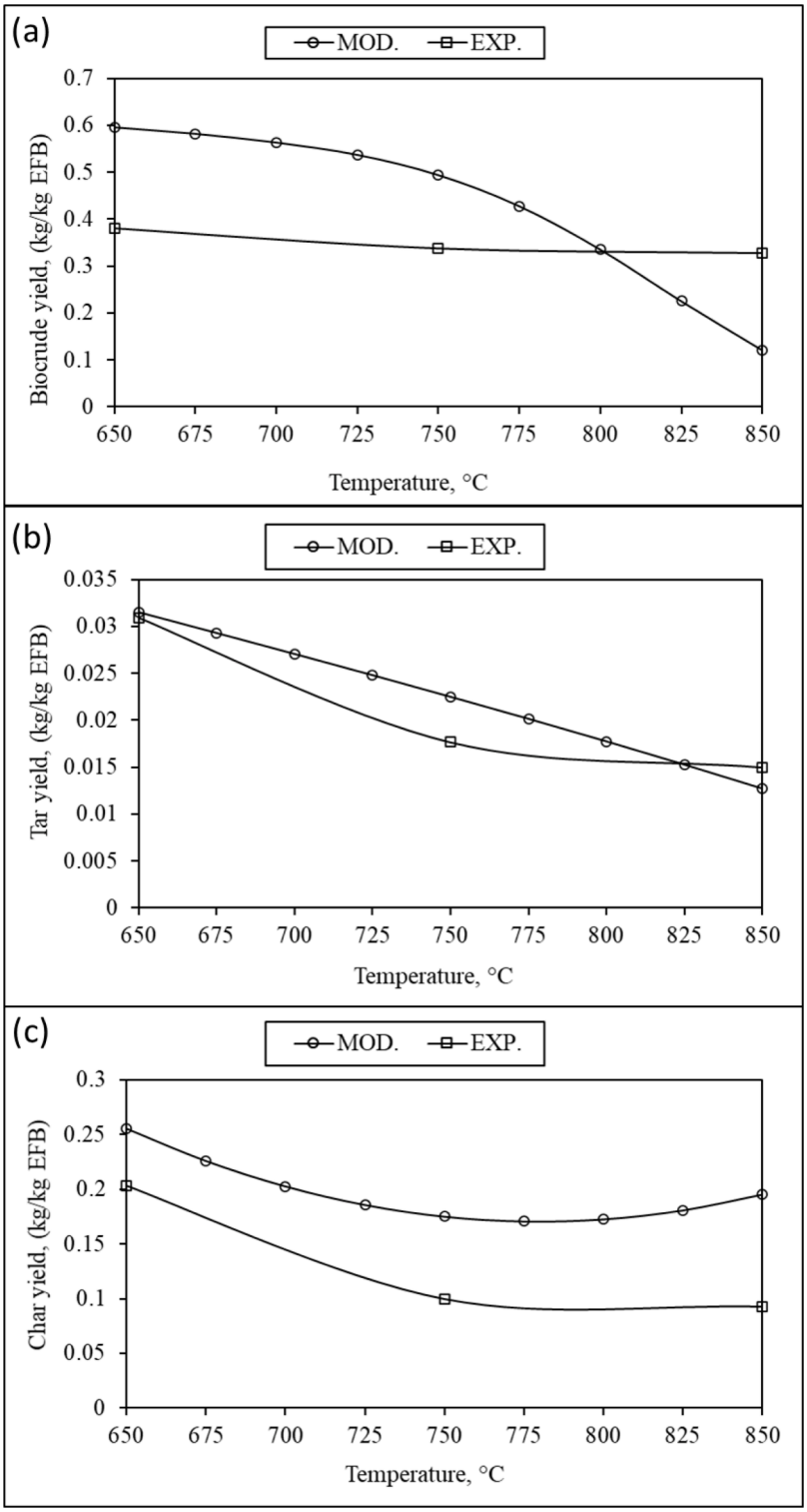

Fig. 8. Model prediction and experimental data of yield (a) biocrude, (b) tar and (c) char.

with a step size of 5 L/min. The yield of H_2 exhibited a 37% increase with increasing the flow rate, as shown in Fig. 11a. Further decomposition of volatiles took place through secondary reactions in case of long residence time [59]. Increasing N_2 flow rate shortens the residence time of gases and retards the change in the extent of tar thermal cracking and shift reactions. Usually, the shift reactions, especially WGSR, consumed the produced H_2 during cracking of tar; consequently, the yield of H_2 reduced. In case of high N_2 flow rates (short residence time), the rate of H_2 consumption through backward reaction of WGSR is minimised due to sweeping of the gases resulting in high concentration of H_2. The study in [60] presented a stable trend while an increasing trend for H_2 was obtained in [61], which explained the effects of gas residence time on the cracking and shift reactions [62].

The yield of CO_2 exhibited a great increase around 69% which was consistent with H_2 yield since both components swept rapidly with increasing flow, as illustrated in Fig. 11b. The experimental work of Gilbert et al. [60] revealed an opposite trend since many of the shift reactions might interact during pyrolysis. In particular, the experiments

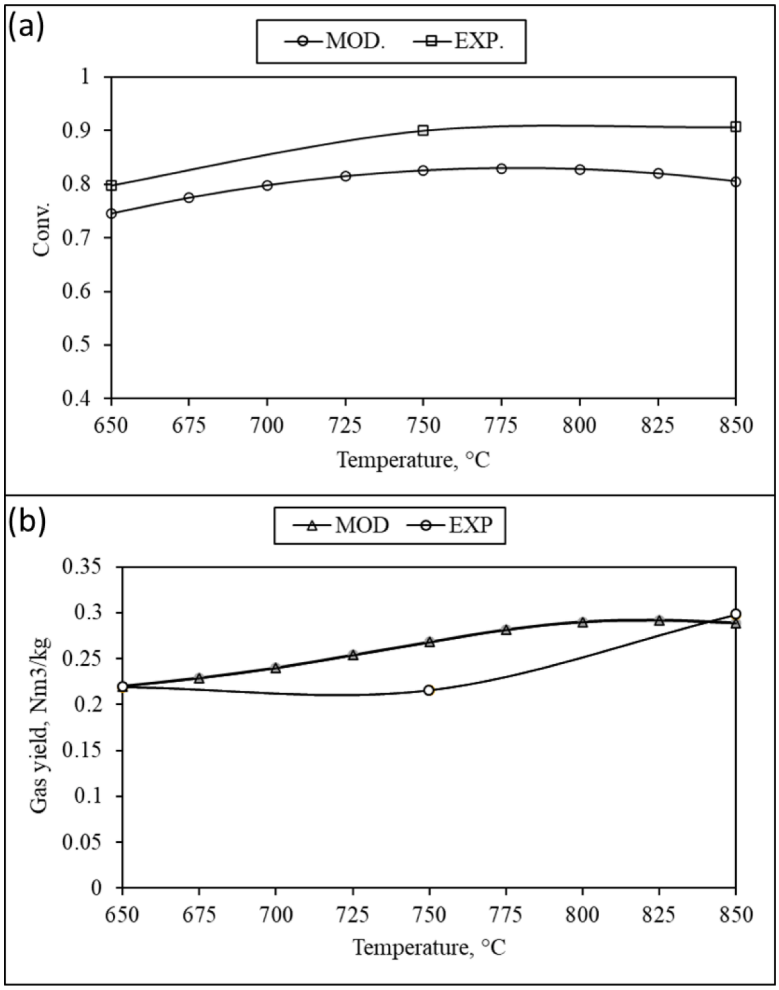

Fig. 9. Experimental results and model predictions on effects of temperature on (a) conversion of EFB and (b) gas yield.

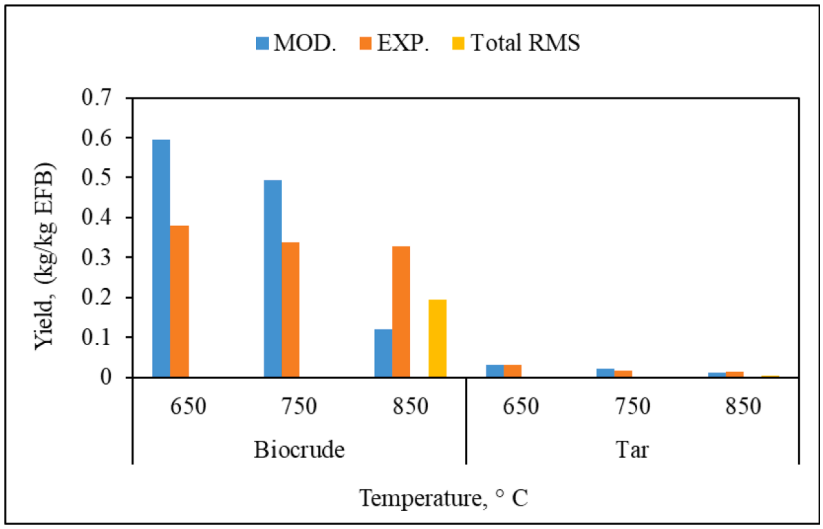

Fig. 10. Comparison between model predictions and experimental results for biocrude and tar yield at different temperatures with calculated RMS.

were carried out over char bed which might increase the interaction between char and CO_2 through Boudouard reaction, resulting in less CO_2 concentration. Furthermore, the model in this study considered only WGSR as one of the main shift reactions. For the same reason mentioned above, the yield of CO decreased progressively by 10.7% with increasing flow because of slowdown of the backward rate in WGSR which resulted in less amount of CO, as shown in Fig. 11c. This agreed well with the study of Gilbert et al. [60] where similar trend was obtained. Meanwhile, the trend of CH_4 slightly rose by approximately 6%, which represented an average increase for temperatures between 650 to 850 °C

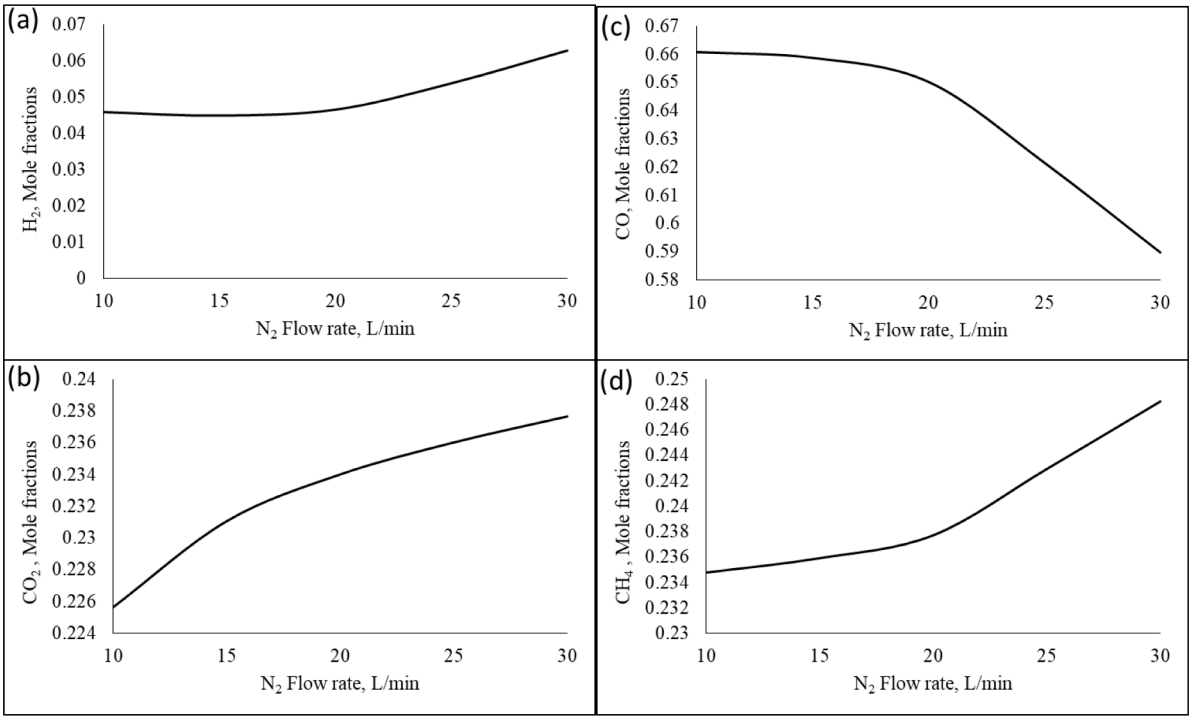

Fig. 11. Effects of N_2 flow rate on (a) H_2, (b) CO_2, (c) CO and (d) CH_4 yield.

and flow range (10 – 30 L/min). The yield of CH_4 yield was presented in Fig. 11d, agreed with that reported by Gilbert et al. [60], while an opposite trend was reported by Yang et al. [61]. These different trends were due to involvement of CH_4 in many shift reactions which resulted in different interactions depending on the experimental conditions. In this study, only steam reforming of CH_4 was considered which revealed no significant conversion at the conditions in the proposed model.

As can be seen from Fig. 12a, the total gas yield (in Nm^3/ kg EFB) decreased with increasing flow rate since less vapours decomposed due to short residence time. This trend was consistent with trends from Abdullah et al. [63], Gilbert et al. [60], and Yang et al. [61]. Conversely, the yield of biocrude increased which demonstrated a grow of 2.1 %, as shown in Fig. 12b. As for tar, the yield increase was small with 0.149%, as illustrated in Fig. 12c. However, less hydrocarbon conversion obtained when flow increased. In the study of Abdullah et al. [63] and Gilbert et al [60]., the bio-oil and tar yield also increased with increasing N_2 flow rate. Finally, the trend of char yield was plateau with increasing flow, as depicted in Fig. 12d. This trend was expected since the carbon

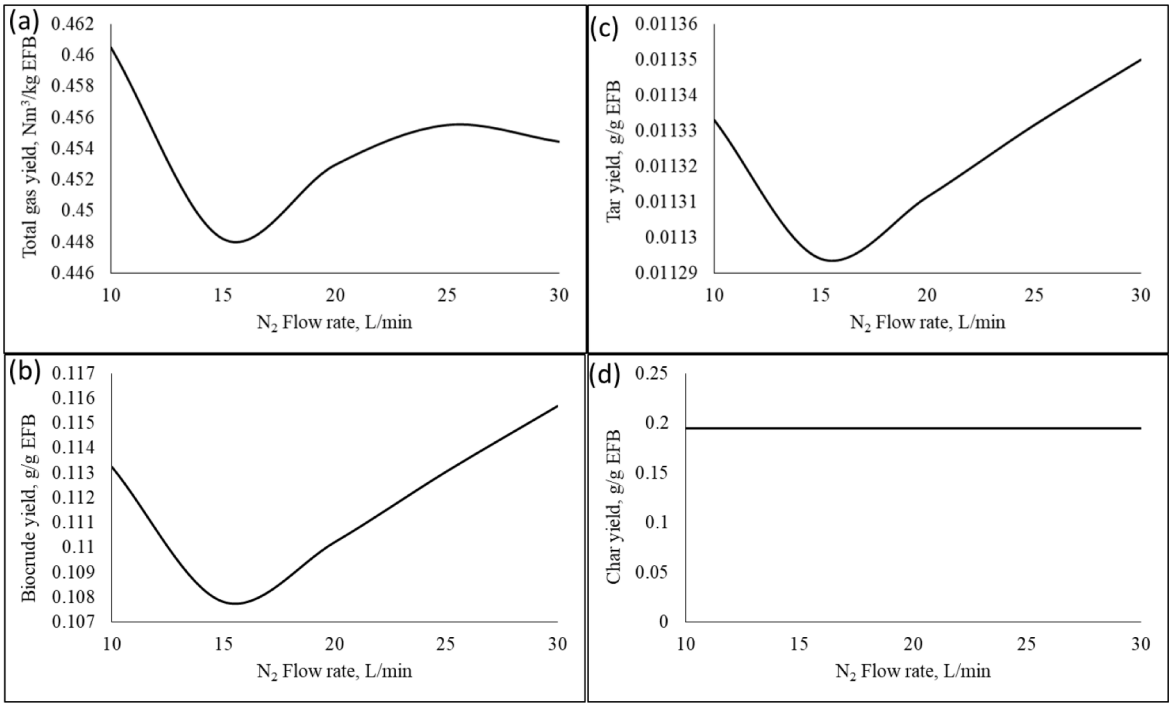

Fig. 12. Effects of N_2 flow rate on (a) total gas, (b) biocrude, (c) tar and (d) char yield.

content of char was subtracted initially from the total carbon produced from devolatilisation of EFB and skipped the homogenous pseudo-equilibrium calculations of gaseous species. Similar trends were obtained by Abdullah et al. [63] and Gilbert et al. [60]. Overall, the model captured the variations on product yield and composition at different process temperatures and N_2 flow rates. The effects of these parameters were noticed on the gaseous components (H_2, CO, and CO_2) through shifting WGSR backward, depending on the conditions. Particularly, the composition of syngas (H_2 and CO) was remarkably changed at different conditions, proving the role of WGSR in devolatilisation process. Moreover, the biocrude and tar also revealed an increase to the flow rate change.

4. Conclusions

A PEM was developed in this for prediction of product yield and composition from devolatilisation of empty fruit bunch. The PEM well predicted the yield of tar with low RMS (0.003), and its conversion (59.7%) compared to experimental work in this study (51.5%). Inclusion of correction factor for SRMR and WGSR is important for better prediction of CH_4, CO, H_2 and CO_2 composition. Fair predictions were obtained for bio-oil and char yields. The predicted carbon in the gas phase agreed well with the experimental results. Yield of tar was significantly affected by temperature rise for temperature range between 650 and 850 °C. Meanwhile, the other devolatilisation products were affected considerably with temperature increase. In contrast, the carrier gas flow rate increases between 10 and 30 L/min revealed less effects on the tar yield, and considerable effects on the WGSR. The model can be used for prediction of yield and composition from devolatilisation of other biomass feedstock. Nevertheless, its reliability requires further validation against the experimental work.

Funding

Authors would like to acknowledge the financial support from Ministry of Higher Education Malaysia via Fundamental Research Grant Scheme (FRGS/1/2020/WAB03/UPM/02/1) and (FRGS/1/2020/TK0/UPM/02/15).

Declaration of Competing Interest

The authors declare that they have no known competing financial interests or personal relationships that could have appeared to influence the work reported in this paper.

Data availability

Data will be made available on request.

References

[1] K.K. Hoo, M.S. Md Said, Simulation of air gasification of Napier grass using Aspen Plus, Sustain. Energy Techno. Assess. 50 (2022), 101837, https://doi.org/10.1016/j.seta.2021.101837.
[2] R.J. Evans, T.A. Milne, Molecular characterization of the pyrolysis of biomass, Energy Fuels 1 (1987) 123–137.
[3] Y. Shen, J. Wang, X. Ge, M. Chen, By-products recycling for syngas cleanup in biomass pyrolysis – An overview, Renew. Sustain. Energy Rev. 59 (2016) 1246–1268, https://doi.org/10.1016/j.rser.2016.01.077.
[4] A. Gómez-Barea, B. Leckner, Modeling of biomass gasification in fluidized bed, Progr. Energy Combust. Sci. 36 (2010) 444–509.
[5] M. Cortazar, L. Santamaria, G. Lopez, J. Alvarez, L. Zhang, R. Wang, et al., A comprehensive review of primary strategies for tar removal in biomass gasification, Energy Conver. Manage. 276 (2023), 116496, https://doi.org/10.1016/j.enconman.2022.116496.
[6] A.K. Vuppaladadiyam, S.S. Varsha, V.S. Vuppaladadiyam, E. Sikarwar, K. K. Ahmad, M.S Pant, et al., A critical review on biomass pyrolysis: Reaction mechanisms, process modeling and potential challenges, J. Energy Instit. 108 (2023), 101236, https://doi.org/10.1016/j.joei.2023.101236.
[7] A. Gagliano, F. Nocera, M. Bruno, I. Blanco, Effectiveness of thermodynamic adaptative equilibrium models for modeling the pyrolysis process, Sustain. Energy Techno. Assess. 27 (2018) 74–82, https://doi.org/10.1016/j.seta.2018.03.006.
[8] S. Srinivas, R.P. Field, H.J. Herzog, Modeling tar handling options in biomass gasification, Energy Fuels 27 (2013) 2859–2873.
[9] B. Zhao, X. Zhang, L. Chen, R. Qu, G. Meng, X. Yi, et al., Steam reforming of toluene as model compound of biomass pyrolysis tar for hydrogen, Biomass Bioenergy 34 (2010) 140–144.
[10] J. Ashok, N. Dewangan, S. Das, P. Hongmanorom, M.H. Wai, K. Tomishige, et al., Recent progress in the development of catalysts for steam reforming of biomass tar model reaction, Fuel Process. Technol. 199 (2020), 106252, https://doi.org/10.1016/j.fuproc.2019.106252.
[11] S. Jarungthammachote, A. Dutta, Thermodynamic equilibrium model and second law analysis of a downdraft waste gasifier, Energy 32 (2007) 1660–1669.
[12] P. Basu, Biomass Gasification And Pyrolysis: Practical Design And Theory, Academic Press, 2010.
[13] C. Di Blasi, Modeling chemical and physical processes of wood and biomass pyrolysis, Progr. Energy Combust. Sci. 34 (2008) 47–90.
[14] H.S.O. Qatan, W.A. Wan Ab Karim Ghani, M.S. Md Said, Prediction and optimization of syngas production from Napier grass air gasification via kinetic modelling and response surface methodology, Energy 270 (2023), 126883, https://doi.org/10.1016/j.energy.2023.126883.
[15] NIST. NIST-JANAF Thermochemical Tables.
[16] H. Ghassemi, R. Shahsavan-Markadeh, Effects of various operational parameters on biomass gasification process; a modified equilibrium model, Energy Conver. Manage. 79 (2014) 18–24.
[17] S. Channiwala, P. Parikh, A unified correlation for estimating HHV of solid, liquid and gaseous fuels, Fuel 81 (2002) 1051–1063.
[18] H. Thunman, Principles And Models Of Solid Fuel Combustion, Chalmers University of Technology, 2001.
[19] NIST. NIST Chemistry WebBook.
[20] D.M. Himmelblau, J.B. Riggs, Basic Principles And Calculations In Chemical Engineering, FT Press, 2012.
[21] N. Abdullah, H. Gerhauser, Bio-oil derived from empty fruit bunches, Fuel 87 (2008) 2606–2613.
[22] S. Jarungthammachote, A. Dutta, Equilibrium modeling of gasification: Gibbs free energy minimization approach and its application to spouted bed and spout-fluid bed gasifiers, Energy Conver. Manage. 49 (2008) 1345–1356.
[23] S. Sadaka, A.A. Boateng. Pyrolysis and bio-oil. 2009.
[24] C. Rubiano, Characterization Of Tar From A Fluidized Bed Steam Reformer Of Black Liquor, The University of Utah, USA, 2006.
[25] A. Gómez-Barea, B. Leckner, Estimation of gas composition and char conversion in a fluidized bed biomass gasifier, Fuel 107 (2013) 419–431.
[26] A. Bridgwater, The production of biofuels and renewable chemicals by fast pyrolysis of biomass, Int. J. Glob. Energy Issues 27 (2007) 160–203.
[27] F. Karaosmanoğlu, E. Tetik, E. Göllü, Biofuel production using slow pyrolysis of the straw and stalk of the rapeseed plant, Fuel Process. Technol. 59 (1999) 1–12.
[28] R. Luque, L. Herrero-Davila, J.M. Campelo, J.H. Clark, J.M. Hidalgo, D. Luna, et al., Biofuels: a technological perspective, Energy Environ. Sci. 1 (2008) 542–564.
[29] H. Fogler, L. Brown, Distributions of Residence Times For Chemical reactors., Elements of Chemical Reaction Engineering, Pearson Education, Indiana, 1992, pp. 708–758.
[30] A. Jess, Mechanisms and kinetics of thermal reactions of aromatic hydrocarbons from pyrolysis of solid fuels, Fuel 75 (1996) 1441–1448.
[31] W. Jones, R. Lindstedt, Global reaction schemes for hydrocarbon combustion, Combust. Flame 73 (1988) 233–249.
[32] J. Manion, R. Huie, R. Levin, D. Burgess Jr, V. Orkin, W. Tsang, et al., NIST Chemical Kinetics Database, NIST Standard Reference Database 17, Version 7.0 (Web Version), Release 1.6. 8, Data version 2013.03, National Institute of Standards and Technology, Gaithersburg, Maryland, 2013, pp. 20899–28320. Web address, http://kineticsnist.gov.
[33] S. Nilsson, Modeling and Simulation of a Three-Stage Gasification Technology for Waste and Biomass, University of Seville, Spain, 2012.
[34] H. William, Numerical Recipes in C: The art of Scientific Computing, Cambridge University Press, 1997.
[35] R. Reschmeier, D. Roveda, D. Müller, J. Karl, Pyrolysis kinetics of wood pellets in fluidized beds, J. Anal. Appl. Pyrol. 108 (2014) 117–129.
[36] C. Di Blasi, C. Branca, Kinetics of primary product formation from wood pyrolysis, Ind. Eng. Chem. Res. 40 (2001) 5547–5556.
[37] B. Wagenaar, W. Prins, W.P.M. van Swaaij, Flash pyrolysis kinetics of pine wood, Fuel Process. Technol. 36 (1993) 291–298.
[38] A. Liden, F. Berruti, D. Scott, A kinetic model for the production of liquids from the flash pyrolysis of biomass, Chem. Eng. Commun. 65 (1988) 207–221.
[39] R. Font, A. Marcilla, J. Devesa, E. Verdú, Kinetic study of the flash pyrolysis of almond shells in a fluidized bed reactor at high temperatures, J. Anal. Appl. Pyrol. 27 (1993) 245–273.
[40] J. Rath, G. Staudinger, Cracking reactions of tar from pyrolysis of spruce wood, Fuel 80 (2001) 1379–1389.
[41] S.R.A. Kersten, R.H.W. Moonen, W. Prins, W.P.M. van Swaaij, Gas mixing in pilot scale (500 kWth) air blown circulating fluidised bed biomass gasifier, in: A. V. Bridgwater (Ed.), Progress in Thermochemical Biomass Conversion, Blackwell Science, CambridgeMA, 2001, pp. 452–464.
[42] J. Sternéus, F. Johnsson, B. Leckner, Gas mixing in circulating fluidised-bed risers, Chem. Eng. Sci. 55 (2000) 129–148.
[43] M.L. Souza-Santos, Solid Fuels Combustion and Gasification, Marcel Dekker, 2004.

[44] B.J. Vreugdenhil, R.W.R. Zwart, Tar Formation in Pyrolysis and Gasification, Energy Research Centre of the Nehterlands, Netherlands, 2009.
[45] P.O. Morf, Secondary Reactions of Tar during Thermochemical Biomass Conversion, Swiss Federal Institute of Technology Zurich, Switzerland, 2001.
[46] V. Skoulou, G. Koufodimos, Z. Samaras, A. Zabaniotou, Low temperature gasification of olive kernels in a 5-kW fluidized bed reactor for H2-rich producer gas, Int. J. Hydrogen Energy 33 (2008) 6515–6524.
[47] C.R. Altafini, P.R. Wander, R.M. Barreto, Prediction of the working parameters of a wood waste gasifier through an equilibrium model, Energy Conver. Manage. 44 (2003) 2763–2777.
[48] R. Karamarkovic, V. Karamarkovic, Energy and exergy analysis of biomass gasification at different temperatures, Energy 35 (2010) 537–549.
[49] K.K. Hoo, M.S. Md Said, Air gasification of empty fruit bunch: an aspen plus model, Bioresour. Technol. Rep. 16 (2021), 100848, https://doi.org/10.1016/j.biteb.2021.100848.
[50] M.S.M. Said, W.A.W.A.K. Ghani, H.B. Tan, D.K.S. Ng, Prediction and optimisation of syngas production from air gasification of Napier grass via stoichiometric equilibrium model, Energy Conver. Manage.: X 10 (2021), 100057, https://doi.org/10.1016/j.ecmx.2020.100057.
[51] H.-M. Yan, C. Heidenreich, D. Zhang, Modelling of bubbling fluidised bed coal gasifiers, Fuel 78 (1999) 1027–1047.
[52] N. Gao, A. Li, Modeling and simulation of combined pyrolysis and reduction zone for a downdraft biomass gasifier, Energy Conver. Manage. 49 (2008) 3483–3490.
[53] M. Becidan, Ø. Skreiberg, J.E. Hustad, Products distribution and gas release in pyrolysis of thermally thick biomass residues samples, J. Anal. Appl. Pyrol. 78 (2007) 207–213.
[54] M.S. Md Said, A.A. Azni, W.A. Wan Ab Karim Ghani, A. Idris, M.F.Z. Ja'afar, M. A. Mohd Salleh, Production of biochar from microwave pyrolysis of empty fruit bunch in an alumina susceptor, Energy 240 (2022), 122710, https://doi.org/10.1016/j.energy.2021.122710.
[55] R. Yan, H. Yang, T. Chin, D.T. Liang, H. Chen, C. Zheng, Influence of temperature on the distribution of gaseous products from pyrolyzing palm oil wastes, Combust. Flame 142 (2005) 24–32.
[56] B. Hosseinzaei, M.J. Hadianfard, B. Aghabarari, M. García-Rollán, R. Ruiz-Rosas, J. M. Rosas, et al., Pyrolysis of pistachio shell, orange peel and saffron petals for bioenergy production, Bioresour. Technol. Rep. 19 (2022), 101209, https://doi.org/10.1016/j.biteb.2022.101209.
[57] T. Chen, H. Liu, P. Shi, D. Chen, L. Song, H. He, et al., CO2 reforming of toluene as model compound of biomass tar on Ni/Palygorskite, Fuel 107 (2013) 699–705.
[58] C. Dupont, J.-M. Commandré, P. Gauthier, G. Boissonnet, S. Salvador, D. Schweich, Biomass pyrolysis experiments in an analytical entrained flow reactor between 1073K and 1273K, Fuel 87 (2008) 1155–1164.
[59] D.S. Scott, J. Piskorz, The continuous flash pyrolysis of biomass, Canad. J. Chem. Eng. 62 (1984) 404–412.
[60] P. Gilbert, C. Ryu, V. Sharifi, J. Swithenbank, Tar reduction in pyrolysis vapours from biomass over a hot char bed, Bioresource Technol. 100 (2009) 6045–6051.
[61] H. Yang, R. Yan, H. Chen, D.H. Lee, D.T. Liang, C. Zheng, Pyrolysis of palm oil wastes for enhanced production of hydrogen rich gases, Fuel Process. Technol. 87 (2006) 935–942.
[62] W.-H. Chen, W. Farooq, M. Shahbaz, S.R. Naqvi, I. Ali, T. Al-Ansari, et al., Current status of biohydrogen production from lignocellulosic biomass, technical challenges and commercial potential through pyrolysis process, Energy 226 (2021), 120433, https://doi.org/10.1016/j.energy.2021.120433.
[63] N. Abdullah, H. Gerhauser, F. Sulaiman, Fast pyrolysis of empty fruit bunches, Fuel 89 (2010) 2166–2169.